Università degli studi di Padova
Facoltà di ingegneria

Bioingegneria

Compartmental Models for the Assessment of Net Whole Body Protein Breakdown Using a Pulse of Phenylalanine and Tyrosine Stable Isotopes in Humans

Candidate:
Alvise Mason

Supervisor:
Prof. Gianna Maria Toffolo

Co-Supervisor:
Prof. Nicolaas EP Deutz

Academic Year 2015/2016

Never say never. Because limits, like fears, are often just an illusion.
Michael Jordan

Abstract

The assessment of whole body amino acid and protein metabolism from tracer kinetic data to describe healthy conditions and disease states has been widely performed for many years by means of primed-constant infusion protocols that only provide limited non-compartmental information. Given the critical and clinical importance of such topic, there is a need for a more accurate, detailed modeling of Phenylalanine (Phe) and Tyrosine (Tyr) metabolism to describe whole body protein synthesis and breakdown in humans, especially as far as pulse protocols are concerned. In this thesis, two compartmental models of Phe and Tyr metabolism in healthy subjects were developed, by using two stable isotope tracer pulses administered intravenously. Kinetic analysis was performed on the three tracer responses in plasma expressed by tracer-tracee ratios and obtained by LC-MS/MS by isotope dilution. The simplest model (Model 1) provides an important and physiologically relevant overview of Phe and Tyr metabolism (in terms of intervals of validity) than the non-compartmental approaches presented in the past. One of the limit case scenarios (Model 1.a) described by this model shows results that are compatible with those found using less structurally complex approaches. Nevertheless, the other limit case scenario (Model 1.b) is likely to be better representative of changes in protein synthesis and breakdown in tissues like muscle, thanks to the development of a more complex and elaborate compartmental model (Model 2). This last model provides accurate estimates for all the unknown parameters, gathers innovative and detailed structural informations for the metabolism of Phe-Tyr kinetics and was validated by using results from a continuous infusion experiment on pigs. The models presented in this thesis could serve not only as a useful reference for a more complete and physiologically based overview of the Phe and Tyr metabolic pathways but they could also guide future developments in the modeling of amino acids characterized by resembling structural properties. By describing the postabsorptive whole body protein kinetics in healthy humans the models provide a direction to accurately and comprehensively assess alterations in whole body protein synthesis and breakdown rates in disease states.

Contents

Introduction

The assessment of whole body amino acid and protein metabolism from tracer kinetic data to describe healthy conditions and disease states has been widely performed for many years by means of primed-constant infusion protocols that only provide non-compartmental information [15, 16, 8, 14, 36, 35]. Only in rare cases this was done by means of compartmental mathematical analysis, usually after a pulse injection [11, 31, 5]. One of the reasons for the limited development of compartmental models that provide a comprehensive, accurate description of amino acid and protein kinetics is the inherited complexity of the system [4], as whole body metabolism needs to be translated to compartments in the body. Tracer non-compartmental approaches currently in use are a good source of information to describe some features of the observed system, but give a limited physiological insight of the structural compartmental characteristics. Unlike the non-compartmental approaches, compartmental modeling involves the postulation of a specific compartmental structure [7]. Compartments must be based on available physiological information, numerical identification from the experimental data and subsequent validation. Given the critical and clinical importance of describing whole body protein metabolism in health and disease, there is a need for a more accurate, elaborate modeling of Phenylalanine (Phe) and Tyrosine (Tyr) metabolism to describe whole body protein synthesis and breakdown in humans [26].

In this thesis the development of two models of Phe and Tyr kinetics is presented, in order to better describe postabsorptive whole body protein kinetics in healthy humans. To do this, a multiple-tracer database was generated and two compartmental models of different complexity were proposed. Both models allow the measurement of important Phe and Tyr kinetic events, including the estimates of the Phe and Tyr involved in the Phe to Tyr conversion, and the conversion flux from Phe to Tyr. The simplest model only provides intervals of validity of the estimates of all the other fluxes and pools, but uses minimal assumptions on the model structure. The more complex model is uniquely identifiable, thanks to some structural assumptions made in the design phase which were validated using results from a continuous infusion experiment on pigs. Both models also allowed the identification of an issue related to the mixing properties of the accessible Tyr pool in the

first minutes after the pulse injection. It is important to point out that non-compartmental approaches cannot address this.
The models presented in this thesis could serve not only as a useful reference for a more complete and physiologically based overview of the Phe and Tyr metabolic pathways but they could also guide future developments in the modeling of amino acids characterized by resembling structural properties. By describing the postabsorptive whole body protein kinetics in healthy humans the models provide a direction to accurately and comprehensively assess alterations in whole body protein synthesis and breakdown rates in disease states.
This thesis is the result of a collaboration between the Department of Information Engineering (DEI), University of Padova and the Center for Translational Research in Aging and Longevity (CTRAL), Texas A&M University. The work was conducted under the combined supervision of Prof. Gianna Maria Toffolo (DEI) and Prof. Nicolaas EP Deutz (CTRAL).

Chapter 1

Background

1.1 Amino Acids and Proteins: General Physiological Notions

At least 30 different amino acids are found in nature. It was thought for some time that only 20 amino acids were present in mammalian, but is now known that there are 21 (being the 21^{st} selenocysteine, Table 1.1). The study of amino acid metabolism is considerably more complex than that of either glucose or lipid, given that the metabolism of each amino acid is different from the others. Nevertheless, a general understanding of the general principles of amino acid metabolism is of great utility. Protein represents the second largest store of chemical energy in the body, but it is not typically used for generating ATP, except from some disease states and extreme conditions (e.g. very sustained exercise, prolonged starvation). The largest deposit of protein in the body is in skeletal muscle (about 40% of total body weight). The synthesis of protein requires amino acids, whereas degradation of proteins produces amino acids and the two processes occur simultaneously. Hence, there is a perpetual turnover of protein, which accounts for 20% of the resting energy expenditure. Free amino acids comprise only 1% of the total amino acid N, which means that 99% of the amino acids in the body is bound in proteins.

1.1.1 Intra and Extracellular Concentrations of Amino Acids in Humans

A general overview of the intracellular concentrations of amino acids in plasma, liver and muscle is shown in Table 1.2, keeping in mind that the values reported by authors in the literature vary slightly.

Table 1.1: The 21 amino acids present in mammalian proteins

	Standard Abbreviation		
Amino acids in proteins	**3-Letter**	**1-Letter**	**Molecular Mass**
Essential (indispensable)			
Histidine	His	H	155
Isoleucine	Ile	I	131
Leucine	Leu	L	131
Lysine	Lys	K	146
Methionine	Met	M	149
Phenylalanine	Phe	F	165
Threonine	Thr	T	119
Tryptophan	Trp	W	204
Valine	Val	V	117
Non-essential (dispensable)			
Alanine	Ala	A	89
Arginine	Arg	R	174
Aspartate	Asp	D	133
Cysteine	Cys	C	121
Asparagine	Asn	N	132
Glutamate	Glu	E	147
Glutamine	Gln	Q	146
Glycine	Gly	G	75
Proline	Pro	P	115
Serine	Ser	S	105
Tyrosine	Tyr	Y	181
Selenocysteine			168

Data from Matthews (2006). The single letter abbreviations are often used to indicate amino acid sequences in proteins. Molecular mass is rounded to the nearest whole number and represents the number of grams per mole of amino acid. Cysteine and Tyrosine are described as conditionally essential amino acids.

Table 1.2: Concentrations of free amino acids in Plasma, Liver and Muscle

	Concentrations (mmol/L)		
Amino acid	**Plasma**	**Liver**	**Muscle**
Alanine	0.36	3.2	3.2
Arginine	0.06	0.03	0.57
Aspartic acid	0.01	18.7	1.0
Asparagine	0.05	0.32	0.40
Cysteine	0.09	-	0.16
Glutamic acid	0.02	4.1	3.8
Glutamine	0.60	5.1	20.0
Glycine	0.20	3.7	1.5
Histidine	0.07	0.77	0.40
Isoleucine	0.05	0.10	0.10
Leucine	0.11	0.30	0.24
Lysine	0.16	0.25	1.2
Methionine	0.02	0.05	0.1
Phenylalanine	0.06	0.10	0.09
Proline	0.22	-	1.6
Serine	0.10	1.0	0.71
Taurine	0.07	8.5	25.0
Threonine	0.11	0.55	0.67
Tryptophan	0.04	0.03	0.1
Tyrosine	0.05	0.15	0.14
Valine	0.21	0.32	0.30

Data from Blomstrand et al. (1995), Matthews (2006), Barle et al. (1996). Values reported by the authors vary slightly. Taurine is a sulphur amino acid, not present in proteins. For the calculation from the amount in fresh (wet) tissue, it is assumed that the intracellular water makes 40% of the weight. The concentrations of selenocysteine have not been measured. The total concentration of all the essential amino acids (without cysteine) is the same in muscle and liver. Similarly the total concentration of all the non-essential amino acids (excluding taurine) is similar.

1.1.2 Sources of amino acids

There are four sources of amino acids that enter the free amino acid pool in the body: proteins in food, proteins secreted into the stomach and intestine by the digestive glands, endogenous proteins and microorganisms that die and release their protein in the colon.

- *Food*: In developed countries, the average daily intake of proteins is approximately 90 g. During digestion, proteins are hydrolyzed to release amino acids that are absorbed into the enterocytes of the small intestine and then enter the blood, from where they are taken up by tissues for peptide and protein synthesis or to enter the pathways of metabolism. Free amino acids are present in food, but the amounts are typically negligible.

- *Small intestine and pancreas*: Daily, about 70 g of protein enter the intestine lumen from secretory cells in the form of digestive enzymes and mucus and from desquamated epithelial cells.

- *Endogenous protein*: The protein turnover process involves hydrolysis of cellular protein, with release of free amino acids into the intracellular compartment.

- *Bacterial and other microorganisms in the intestine*: These are present mainly in the colon. Death of the microorganisms is followed by their digestion and the release of amino acids into the lumen. The amino acids are then available for use by other microorganisms, by the colonocytes or the liver, after their uptake from the lumen. The use by the liver is quantitatively significant in some conditions.

1.1.3 Protein Turnover

Protein turnover in an adult is approximately 4 to 5 g per kg body weight, which equals about 250 to 350 g of protein hydrolyzed and resynthesized in the tissues of an adult human on a daily basis. This number represents significantly more protein than what is ingested in food. Depending on the nature of the protein, the condition of the subject and the tissue considered, the rates of protein turnover vary enormously. Proteins (mainly enzymes) in the liver are replaced every few hours/days whereas structural proteins (e.g. contractile proteins, collagen) are stable for several months. Under some particular conditions, contractile proteins can be degraded relatively rapidly.
There are two main reasons for protein turnover. First, abnormal proteins can arise in cells because of spontaneous denaturation, errors in protein synthesis/translational processing and failure of the correct folding of the protein or damage by free radicals. They are then degraded and replaced

by newly synthetized proteins. Secondly, turnover helps keeping stable the concentration of free amino acids both within cells and in the blood, which is fundamental to satisfy the requirements for synthesis of essential proteins and peptides (e.g. hormones).
Turnover is a large-scale substrate cycle, whose role (among others) is to regulate the concentration of specific proteins. Hence, the turnover rate of enzymes that control metabolism should be highest, since their activity and therefore concentration is of key importance in the regulation of metabolism. The greatest sensitivity of control, which relates to the greatest precision provided by a cycle, is achieved when there is a high rate of cycling compared to the net rate of synthesis or degradation. Also, the rate of protein turnover is directly proportional to the rate of energy expenditure (i.e. energy expenditure depends partially on rates of protein turnover).
The three pathways responsible for intracellular protein degradation are: the lysosomal-autophagic, ubiquitin-proteasome and calpain-calpastatin system. Although hydrolysis of the peptide bonds does not involve ATP, the various processes of protein degradation require considerable expenditure of energy, possibly more than is required for protein synthesis. Nevertheless, the control of the protein degradation process is very little known, whereas much is known about the control of protein synthesis.

1.1.4 Defects in protein degradation and diseases

When a protein is lost, it must be replaced in order to maintain health: excessive loss contributes to death (typically directly caused by infection or heart failure), as it happens during prolonged starvation or cachexia. In the elderly, trauma, major surgery or poor nutrition can result in loss of so much skeletal muscle that normal daily activities (e.g. walking, climbing stairs, dressing, etc.) are impaired. Due to the important role of the proteasomal-ubiquitin system in the degradation of cellular proteins or proteins of pathogens, any defect in this system could result in disease. Indeed, the accumulation of insoluble proteins that form aggregates in neurons (caused by impaired proteolytic digestion of proteins) is suspected to be one of the possible triggering reasons for some neurodegenerative diseases (e.g. Alzheimer's, Parkinson's, spongiform encephalopathies and motor neuron diseases). Furthermore, failure to control the rate of degradation of cyclins could lead to their over-expression, resulting in an increased risk of tumor development.

1.1.5 Essential and non-essential amino acids

For protein synthesis to take place, all the amino acids must be available within the cell. To this extent, all amino acids are essential. Nevertheless, animal studies have demonstrated that some amino acids are essential for

maintaining nitrogen balance and growth, whereas others are not. This led to the division between essential and non-essential amino acids. The terms indispensable and dispensable are also used, but the difference in their meaning is important. From a biochemical standpoint, non-essential amino acids are those for which a synthetic pathway is present in the body, which is of sufficient capacity to satisfy the normal requirement. On the contrary, essential amino acids are those for which a synthetic pathway is not present. In nutritional terms, dispensable amino acids are defined as those that can be excluded from the diet without affecting nitrogen balance, whereas indispensable amino acids, when excluded from the diet cause negative nitrogen balance. A negative nitrogen balance (more nitrogen is lost than ingested) is typical in conditions such as malnutrition, starvation or in some diseases. A method for determining whether an amino acid is indispensable, it is omitted from the diet while all the others are included. If the omission results in negative nitrogen balance, the amino acid is deemed indispensable. If, because of the absence of this single amino acid, the body has been unable to synthetize proteins, the nitrogen that would have been used in this synthesis is excreted. According to this approach, the following amino acids are considered to be indispensable for humans: isoleucine, leucine, lysine, methionine, phenylalanine, threonine, tryptophan and valine. Histidine used to occupy an in between situation, but more recent studies (powered by novel approaches) have demonstrated that it can be included in the list of essential amino acids. The non-essential amino acids are alanine, arginine, aspartate, asparagine, cysteine, glutamate, glutamine, glycine, proline, serine and tyrosine. A summary of the reactions involved in their synthesis is given in Figure 1.1.

Since the distinction between essential and non-essential amino acids is not always clear-cut, some amino acids become essential only under certain conditions. The rates of synthesis of some amino acids (glutamine, cysteine and possibly glycine and arginine) that are normally considered indispensable is not sufficient under conditions when their demand is increased (e.g. during sepsis, after severe trauma or major surgery). Therefore, the essential nature of these amino acids is conditional. Tyrosine and cysteine can be synthetized from phenylalanine and methionine, respectively. Given that both phenylalanine and methionine are indispensable amino acids, if they are not present in the diet at or below minimal requirement, then there is not sufficient to synthetize tyrosine or cysteine. For this reason, in such scenario these amino acids become indispensable, i.e. conditionally essential.

1.1.6 Fate of amino acids

The three major fates of amino acids are three:

- *Synthesis of new proteins for growth or repair.* The rate of protein

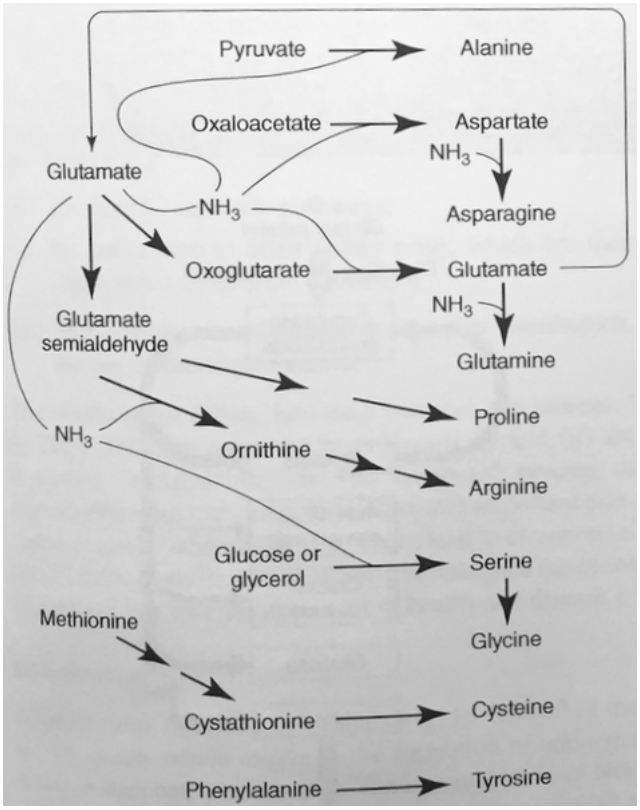

Figure 1.1: A summary of pathways involved in the synthesis of non-essential amino acids

synthesis is a major factor determining the overall rate of amino acid metabolism: the higher its value, the lower the amino acid concentration, which eventually reduces the rate if catabolism.

- *Synthesis of a range of nitrogen-containing small compounds.*

- *Catabolism.* This results, eventually, in formation of ammonia and small carbon-containing compounds. The carbon skeletons are used for the synthesis of glucose and triacylglycerol or for a complete oxidation to carbon dioxide with the generation of ATP. The ammonia is later converted in urea.

1.1.7 Transport of amino acids into the cell

The metabolism of amino acids takes place within the cell but, before this can occur, these need to be transported across the plasma membrane. This requires transport proteins, which have three important characteristics:

- Since the intracellular concentration of most amino acids is considerably higher than that in plasma, the transport of these amino acids requires energy. This is achieved via the Na+ gradient across the plasma membrane, maintained with the usage of ATP.
- There are ten transporters so that some transport more than one amino acid.
- The properties of some transporters are different in different tissues.

1.1.8 Changes in amino acid metabolism in different conditions

The fed state

The protein in the food is digested and the resultant amino acids are absorbed from the intestine: these will be used for synthesis of protein and some nitrogen-containing compounds. Amino acids not required for these two processes are converted to oxoacids, of which about the half are oxidized for ATP generation and the other half is converted to glucose (or glycogen); the ATP generated in the oxidation is used in the conversion to glucose.

Starvation

If starvation lasts for more than 24h, the rate of degradation of body protein exceeds the rate of protein synthesis. The resultant amino acids are converted to oxoacids, most of which are converted to glucose which is released and used predominantly by the brain. In this condition, the ATP required for gluconeogenesis is obtained from the oxidation of fatty acids.

Trauma, surgery and cancer

In these conditions, in general, the rate of degradation of body protein is accelerated and the resultant oxoacids are converted to glucose or are oxidized. If anorexia is present and the patient is not receiving parenteral nutrition, oxoacids will be converted mainly to glucose. The synthesis of some nitrogen-containing compounds is increased for these compounds and the peptides that are required in this condition (e.g. glutamine, arginine, cysteine, cytokines, acute phase proteins).

This brief overview is over-simplified but serves to illustrate the central role played by the changes in amino acid metabolism in the essential physiological processes in these conditions. Some amino acids are metabolized in tissues other that the liver and description of this metabolism provides a more realistic picture of whole-body protein and amino acid metabolism in the body.

1.1.9 Amino acid metabolism in different tissues

Amino acid metabolism is important in all tissues/organs but some of them play a key metabolic role

Liver

The liver is the only organ capable of catabolizing all amino acids, with the important exception of the branched chain amino acids. This makes physiological sense, since it is the only organ in which ammonia can be converted into urea and, furthermore, most amino acids that are absorbed by the gut enter the hepatic portal vein for immediate passage through the liver. In fact, the liver normally removes and catabolizes more than 70% of the amino acids that enter this vein. Nevertheless, on a low protein diet, a lower percentage (especially the essential amino acids) is removed, so that they are available for other tissues. In general, the liver plays a central role in the regulation of catabolism of amino acids.
In order to ensure the protection from degradation of the essential amino acids, with a minimal protein diet, the maximal activities of the enzymes responsible for the degradation of these amino acids are low. As the intake of dietary protein increases, the activities of these enzymes increase, due to acute changes in activity and chronic increases in the amount of enzyme. Acute regulation of essential amino acid oxidation is achieved via changes in amino acid concentrations in tissues. The rate of urea production is also directly proportional to protein intake. This is consistent with the view that the intracellular concentrations of amino acids play a role in the control of the rate of catabolism of amino acids (with consequent formation of ammonia and urea).
The overall rate of amino acid metabolism depends on:

- The concentration of amino acids in the liver
- The activities of the key enzymes that catalyze degradation of the essential amino acids
- The rate of protein synthesis, in liver and other tissues, which depends on the concentrations of some hormones and the concentrations of 'signal' amino acids

Skeletal muscle

The major role of skeletal muscle is movement. Nevertheless, since muscle comprises 40% of the body, it is large enough to play a part in control of the blood concentrations of the major fuels: glucose, fatty acids, triacylglycerol and some amino acids. Skeletal muscle contains the largest quantity of

protein in the body, which is used as a source of amino acids under various conditions (e.g. starvation, trauma, cancer).

1.2 Phenylalanine and Tyrosine in the postabsorptive state: measurement importance and previous proposed models

The principal reason to measure rates of Phenylalanine (Phe) and Tyrosine (Tyr) kinetics in humans is to understand the derangements of the metabolism of these amino acids that occur in patients with the in-born error phenylketonuria (PKU) and in diseases that affect their metabolism, such as in liver or renal disease. PKU is the deficiency of the enzyme Phe hydroxylase (PAH), which is responsible for the conversion of Phe to other essential compounds in the body (Figure 1.2), in particular Tyr. This is a conditionally essential amino acid for PKU patients, because without PAH it cannot be produced in the body through the breakdown of Phe. Tyr is necessary for the production of neurotransmitters like epinephrine, norepinephrine and dopamine. Phe, being an essential amino acid, is a necessary part of the human diet and it is naturally present in all kinds of dietary protein (it is also used to make aspartame, a sweetener). In healthy subjects, the PAH enzyme breaks down any excess of Phe beyond what is needed by the body. However, an insufficiency of the PAH enzyme or its cofactor cause the building up of Phe in the blood and in the brain to toxic levels, affecting brain development and function.

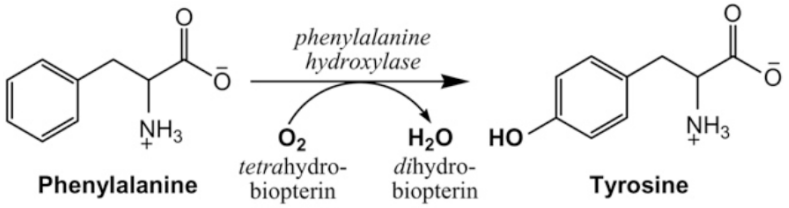

Figure 1.2: The reaction converting Phe to Tyr via PAH

Other than that, Phe and Tyr also have specific characteristics as amino acids that make them useful as markers of protein metabolism. As previously mentioned, they are both indispensable amino acids, which are essential to the diet. In the postabsorptive state, there is no entry of amino acids from dietary sources and the flux of Phe in the body is derived from entry of Phe released from protein breakdown. Such input is matched by Phe removal via protein synthesis and via metabolic disposal by conversion to Tyr. Therefore, in the postabsorptive state the measurement of the rate of appearance of Phe in plasma is an indicator of the whole body rate of proteolysis, while the measurement of the conversion rate (hydroxylation flux) of Phe to Tyr is an index of the net whole body protein breakdown. Additional reasons for determining Phe and Tyr kinetics are the determination of dietary require-

ments of these amino acids and the production of Tyr from dietary Phe.
Prior to 1940, there was only circumstantial evidence that Tyr was produced from Phe, even though authors like Shambaugh, Lewis and Tourtellotte [33] suggested that Phe was not converted to Tyr. In 1940, a study performed by Moss and Schoenheimer [28] on rats provided the key evidence on the conversion and ended the speculation about the metabolism of Phe. Rittenberg, whose model used ^{15}N-labeled amino acids to determine rates of whole body protein synthesis in humans, did the very first kinetic study in the 1950s [32] but many argued on the too many assumptions and limitations of this approach [20].
What quickly became clear from studies in the 1960s was that measurement of whole body protein synthesis using tracers is actually very difficult. In contrast, whole body protein breakdown is easy to measure using an indispensable amino acid tracer. This is due to the concept that the dilution of the indispensable amino acid tracer in blood occurs due to release of unlabeled indispensable amino acid from protein breakdown and entry from the diet [22]. Knowing the rate of indispensable amino acid intake in fed studies or neglecting this route in postabsorptive subjects, the rate of protein breakdown is readily calculated from the dilution of an intravenously infused indispensable amino acid tracer. The first time an indispensable amino acid was used to measure whole body protein breakdown is dated 1967, in a study performed by James et al. [21] using ^{14}C-Lysine. However, it was not until 1988 that Darmaun et al. [17] used a $^{2}H_5$-Phe tracer to measure Phe kinetics and whole body protein breakdown. Waterlow et al. [21] tried to use a ^{14}C-Tyr tracer in 1976, but the use of Tyr tracers is an inherently problematic affaire when measuring whole body protein breakdown, due to the unknown amount of Phe converted to Tyr that also provides an input.

1.2.1 Curtius et al. (1972, 1978) [15, 16]

The early principal use of a deuterated Phe tracer was to assess the conversion of Phe to Tyr, rather than measuring whole body breakdown. Provided that in normal conditions considerable amounts of Phe are converted to Tyr, Phe to Tyr conversion is very limited in PKU patients. Curtius et al. [15] used a ^{2}H-Phe tracer administered in 1 patient as a proof of concept of this method in 1972 and in 1978 followed up this report by measuring Phe to Tyr conversion in PKU and hyperphenylalanemic patients [16]. The approach used by Curtius and al. [15] is shown in the model of Figure 1.3.

The key measurement gleaned here is the enrichment of plasma ^{2}H-Tyr derived from the conversion of the [phenyl-$^{2}H_5$]-Phe tracer normalized against the plasma ^{2}H-Phe enrichment. This Tyr/Phe enrichment ratio defines the fraction of free Tyr that is produced from Phe, which in normal postabsorptive humans should be 15% (given that in this condition 15% of

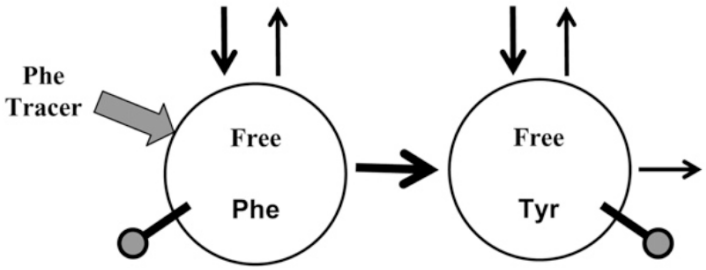

Figure 1.3: The model developed by Curtius et al. [15, 16]

Circles denote the free phenylalanine (Phe) and tyrosine (Tyr) pools. Arrows indicate rates of appearance and disappearance from the free pools due to whole body protein synthesis and breakdown. The wide arrow indicates administration of a Phe tracer (usually by continuous infusion) into the free Phe pool. Tracer abundance (enrichment) is measured in free Phe and in Tyr (indicated by the ball and stick figure to denote sampling from the free pools). The ratio of the Tyr tracer enrichment divided by the Phe tracer enrichment defines the fraction of free Tyr derived from Phe.

indispensable amino acids are oxidized) [22]. Since a PKU patient is expect to have undetectable amounts of ^{2}H-Tyr in plasma following the administration of a ^{2}H-Phe tracer, values between 0 and 15% have been used to classify the degree of impairment in patients with derangements of Phe metabolism [25]. Nevertheless, the very limited capacity of conversion in most PKU patients made the method very difficult to apply with sufficient accuracy in PKU due to the low enrichment of ^{2}H-Tyr.

1.2.2 Clarke and Bier (1982) [8]

Rather than using Phe tracer conversion to Tyr in order to assess derangements of Phe metabolism, Clarke and Bier [8] used the conversion to define normal metabolism. As previously addressed, Tyr can become a conditionally indispensable amino acid when the availability of Phe (due to limited intake) is limited for production of Tyr. Therefore, Tyr synthesis in the body depends upon Phe availability. In a slightly different way to what was done by Curtius et al. [15, 16], Clarke and Bier's model needs also the continuous infusion of a Tyr tracer in order to determine Tyr flux and define the absolute amount of Tyr produced from Phe: they infused a [1-^{13}C]-Tyr tracer in conjunction with the [phenyl-$^{2}H_5$]-Phe tracer to measure simultaneously the turnover rates of both Phe and Tyr as well as the rate of Phe conversion to Tyr. The model for this approach is shown in Figure 1.4.

At the isotopic steady state, the following equations provide the calcula-

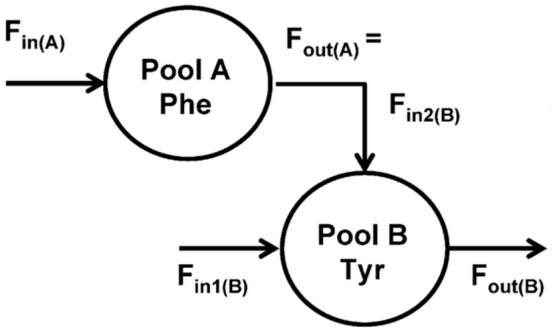

Figure 1.4: The model developed by Clarke and Bier [8]

tions for the variables of the model (Figures 1.4 and 1.5):

$$E_{(A)} = \frac{i_{n(A)}}{F_{in(A)}} \tag{1.1}$$

$$E_{(B)} = \frac{i_{n(B)}}{F_{in(B)}} \tag{1.2}$$

$$E_{(B \leftarrow A)} = E_{(A)} \frac{F_{in2(B)}}{F_{in(B)}} \tag{1.3}$$

$$F_{in2(B)} = \frac{E_{(B \leftarrow A)}}{E_{(B)} F_{in(B)}} \tag{1.4}$$

$$F_{out(A)} = F_{in2(B)} \tag{1.5}$$

$E_{(A)}$ and $E_{(B)}$ are the tracer enrichments in plasma of Phe and Tyr, respectively. $E_{(B \leftarrow A)}$ is the enrichment for the Phe tracer in Tyr. $F_{in(A)}$ and $F_{in(B)}$ are the input fluxes of Phe and Tyr from protein breakdown (rate of appearance in plasma). $i_{n(A)}$ and $i_{n(B)}$ are the the rates of infusion of the Phe and Tyr tracers. Phe disposal ($F_{out(A)}$) is by conversion to Tyr and this rate equals the rate of Tyr production from Phe ($F_{in2(B)}$). Tyr is removed via Tyr degradation ($F_{out(B)}$). Phe has 1 input; Tyr has 2 with the total input being $F_{in(B)} = F_{in1(B)} + F_{in2(B)}$. This model assumes that only the entry of unlabeled Phe and Tyr dilutes the tracers, therefore rates of Phe and Tyr uptake for protein synthesis do not affect tracer enrichments (and for this reason do not appear in the model).

1.2.3 Cortiella et al. (1992) [14]

The only rate left unsolved in Clarke and Bier [8] model is the rate of tyrosine oxidation ($F_{out(B)}$). The normal approach to measure whole body oxidation

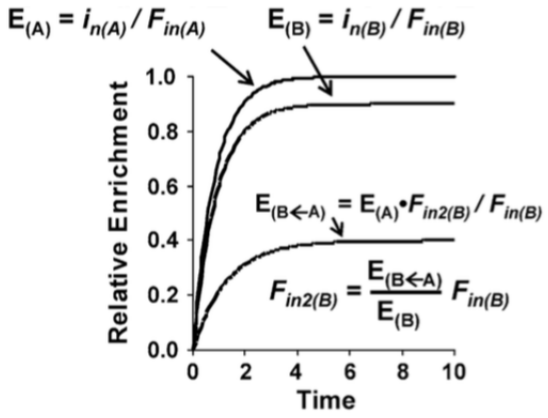

Figure 1.5: Theoretical time courses of the tracer enrichments for Phe ($E_{(A)}$), tyrosine ($E_{(B)}$), and the Phe tracer in Tyr ($E_{(B\leftarrow A)}$)

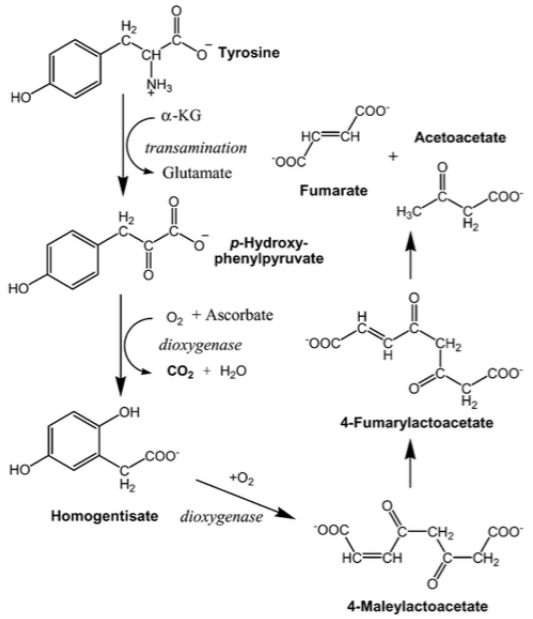

Figure 1.6: Pathway of Tyr degradation.

of a tracer would be to use a ^{13}C or ^{14}C that can be recovered in exhaled CO_2. Figure 1.6 shows the metabolic pathway of Tyr degradation.

The carboxyl carbon of Tyr is almost immediately released as CO_2 during Tyr degradation, the remainder of the molecule either ends up as fumarate or acetoacetate. Even though both molecules may enter the tricarboxylic acid cycle and the label recovered as CO_2, there are also alternative non-oxidative fates. For this, a carbon label placed in the phenyl ring of Tyr will

have a lower recovery in CO_2 than a carbon isotope placed in the carboxyl position. A carboxyl-label is available as the non-radioactive [1-^{13}C]-Tyr, making it the preferred label for measuring Tyr oxidation.
The first reported use of the [1-^{13}C]-Tyr label for oxidation was the work of Cortiella et al. [14] in 1992 who also used a [1-^{13}C]-Phe label to measure Phe oxidation as well. Two series of experiments were performed: one where 6 subjects were continuously infused with [1-^{13}C]-Phe and [2,2-$^{2}H_2$]-Tyr on day 1, and another where they were continuously infused with [2,2-$^{2}H_2$]-Phe and [1-^{13}C]Tyr. In both cases, exhaled $^{13}CO_2$ was determined to define the rate of ^{13}C-tracer oxidation. The key results of this study are summarized in Figure 1.7. The Phe flux was determined from the dilution of Phe tracer in plasma. Tyr flux was determined in a similar way, but its flux is the sum of Tyr from protein breakdown and Tyr from Phe hydroxylation. The rate of Phe hydroxylation was determined for each tracer pair from the Phe tracer appearing as Tyr as described by Clarke and Bier. The oxidation rates of Phe and Tyr were determined from the recovery of tracer as $^{13}CO_2$ in exhaled air.

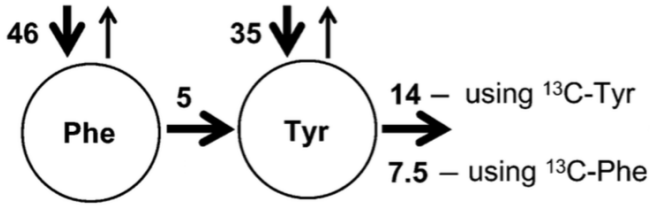

Figure 1.7: The results of Cortiella et al. [14] model

Phe flux is represented by the bold arrow entering the free Phe pool. Tyr flux is the sum of the 2 bold arrows entering the free Tyr pool (Tyr from protein breakdown and Tyr from Phe hydroxylation). Tyr oxidation is represented by the bold arrow exiting the free Tyr pool. All values are reported as μmol·kg^{-1}·h^{-1} and are approximate, because results from the 2 groups of infusions have been combined.

The results (Figure 1.7) of this study are important because they highlight some general points. As already mentioned, in the postabsorptive state the appearance rate of indispensable amino acids into plasma will be proportional to the rate of protein breakdown and the abundance of each amino acid in protein. For instance, leucine is more than twice as abundant as Phe in protein on a molar basis and the leucine whole body flux should be more than double the Phe flux. This relation has been shown in general to be linear for dispensable amino acids [22]. On this basis, we would expect the rate of Tyr to be ∼60% that of Phe. According Cortiella et al. [14] study, this percentage is around 76% (46 and 35 μmol·kg^{-1}·h^{-1} for the Phe and

Tyr fluxes from protein breakdown, respectively). We would expect based upon measurements of indispensable amino acids using ^{13}C or ^{14}C tracers in postabsorptive humans that oxidation should be in the range of 15 to 20% of the flux, which should be 7-9 $\mu mol \cdot kg^{-1} \cdot h^{-1}$ in this case. Instead, the value reported by Cortiella et al. is ~ 5 $\mu mol \cdot kg^{-1} \cdot h^{-1}$. As far as the Tyr oxidation rate from the ^{13}C-Tyr tracer is concerned, we would expect this value to be ~ 6 $\mu mol \cdot kg^{-1} \cdot h^{-1}$ based upon the Tyr appearance rate from protein breakdown (35 $\mu mol \cdot kg^{-1} \cdot h^{-1}$) and the previously anticipated obligatory oxidation of amino acids in the postabsorptive state. To be fair, Phe that must be oxidized via Tyr (estimated to be ~ 8 $\mu mol \cdot kg^{-1} \cdot h^{-1}$) should be added to the amount, for a total expected Tyr oxidation rate of ~ 14 $\mu mol \cdot kg^{-1} \cdot h^{-1}$. This expected value for Tyr oxidation in this case agrees with the measured value for Tyr oxidation.

At this point is important to observe that the rate of Phe hydroxylation was probably underestimated, allegedly due to the use of ^{13}C as a label for Phe. Indeed, if one observes the rate reported in this study for Phe oxidation measured by recovery of the [1-^{13}C]-Phe label in exhaled air (~ 7.5 $\mu mol \cdot kg^{-1} \cdot h^{-1}$), it would look higher than the rate determined for Phe hydroxylation (~ 5 $\mu mol \cdot kg^{-1} \cdot h^{-1}$). This could be due to the fact that the release rate of ^{13}C-Phe tracee has to be underestimated by trapping of ^{13}C label as ^{13}C-Tyr in newly synthetized protein. Therefore, adjusting the rate of Phe hydroxylation upwards would reduce the rate of Tyr entering from protein breakdown toward the expected amount.

Concluding, a complete picture of Phe-Tyr metabolism can be accomplished with 2 tracers (a Phe and a Tyr tracer) and measurement of the Phe tracer in Tyr. Although a [1-^{13}C]-Tyr tracer is ideal for determining Tyr kinetics because one would get also a direct measurement of Tyr oxidation, it may not necessarily be used when combined with a Phe tracer. Although [phenyl-$^{2}H_5$]-Phe is an obvious cheap choice as a tracer, it may produce a significant isotope effect during the conversion to [$^{2}H_4$]-Tyr, making this tracer suboptimal for measuring Phe hydroxylation. Therefore, a [1-^{13}C]-Phe becomes the desired choice, forcing the use of a [2,2-$^{2}H_2$]-Tyr tracer and forfeit of a Tyr oxidation rate measurement.

Because Phe is an indispensable amino acid, its flux provides a good representation of whole body protein breakdown. One of the more consistent uses of Phe tracers has been measurement of rates of protein breakdown in the whole body and in tissues that do not hydroxylate Phe, as muscle. There are a limited number of indispensable amino acids whose metabolism and availability of tracers coincide for use of determining protein kinetics in humans: Phe and Tyr tracers are of key importance in this regard .

1.3 The need for pulse-based protocols and compartmental modeling

All the previously presented models for the measurement of Phe-Tyr metabolism kinetics involved the use of the stable isotope unprimed/primed constant (or continuous) infusion protocols. These protocols are in general quite tough to perform, because a lot of time is typically required to achieve the isotopic plateau at which the kinetic variables can be gleaned. In particular, in the case of the unprimed constant infusion, this amount of time can become extremely high. As far as the primed constant infusion is concerned, the estimation of the priming dose (that allows to achieve the isotopic steady state faster) is often odd. Moreover, constant infusion protocols require accurate infusion pumps, able to infuse consistent amounts of tracer that overall turn out to be particularly expensive.
In this perspective, pulse-based protocols can lead to great savings in terms of time and economic resources needed for the study. First of all, the intravenous injection of the stable isotope tracer solutions can be performed directly by nurses, instead of a way more expensive infusion pump. Then, the amount of tracer is much lower than what is overall required with the constant infusion protocols, leading to relevant savings in terms of money. Aside from the more packed sampling schedule needed, the pulse approach provides the serious overall advantage of a shorter study time. Nevertheless, the calculations necessary to obtain the kinetic variables of the observed metabolic pathway with the pulse approach include a higher computational complexity, due to the need for integrating areas under the curve [36].
Even when these calculations are performed with optimal procedures, the obtained variables can only provide a limited physiological insight in the metabolism. For instance, in the postabsorptive state the rate of appearance in plasma of an amino acid is commonly adopted as a measurement of the whole body protein breakdown. Of course, this is an approximation, because what appears in plasma is only a limited portion of the total amount of that amino acid when it is broken down from proteins in tissues [36]. Moreover, most kinetic aspects characterizing amino acid pathways still remain unknown, especially in the human. The much improved quality of the data produced in the last few years suggests that it is time to develop novel, more reliable and higher in complexity compartmental models of measurement for amino acid kinetics. These models' aim is to eventually improve the quality of the gleaned kinetic variables, together with a deeper physiological insight in the metabolism of amino acids. In fact, only in rare cases the compartmental analysis was applied to amino acid research [11, 31, 5]. One of the reasons for that might be the inherited complexity of the system [4], as whole body metabolism needs to be translated to compartments in the body, together with the limited quality of the data in the past.

For these reasons, in this work a multiple-tracer database was generated with a single pulse-injection protocol and two compartmental models of different complexity for the assessment of Phe-Tyr metabolism were formulated and tested on the dataset.

Chapter 2

Methods

2.1 Dataset

The dataset is a courtesy of the Center for Translational Research in Aging and Longevity (CTRAL), Texas A&M University and was obtained as part of the OCERA Study.

2.1.1 Study Population: anthropometric data and body composition

The study population consisted of 11 healthy subjects (Table 2.1). The subjects were recruited via flyers in the local community and subsequently screened. Written informed consent was obtained from all subjects and the study was approved by the Institutional Review Board, Texas A&M University.
Body weight was measured by a digital beam scale and height by a stadiometer. Whole body fat-free mass (FFM) was obtained by dual-energy X-ray absorptiometry (Hologic QDR 4500/ Version 12.7.3.1 (Bedford, MA)).

2.1.2 Study protocol

All subjects were studied at the Clinical Research Unit of the Center for Translational Research in Aging and Longevity, Texas A&M University. The study day started in the early morning after an overnight fast and lasted for approximately 3 hr. A solution (8.1 mL vol) that contained the stable isotopes of L-[ring-$^{13}C_6$]-Phe (37 mM) and L-[ring-$^{2}H_4$]-Tyr (2.5 mM) was prepared (Cambridge Isotope Laboratories (Woburn, MA, USA)). The solution was made iso-osmolar (300 mOsm) by adding NaCl. Body weight, height and vital signs were measured, and a peripheral line was placed in an antecubital vein of the arm for infusion of the stable isotopes (Table 2.1). A second catheter for arterialized venous blood sampling was placed in a superficial dorsal vein of the hand or lower arm of the contralateral arm. The

Table 2.1: Subject Characteristics

Subject (ID)	Gender	Age	BW (kg)	FFM (kg)	FFM (%BW)	$Dose_{Phe+6}$ (μmol)	$Dose_{Tyr+4}$ (μmol)
A	M	55	87.2	65.1	75	301.224	20.049
B	F	56	91.3	50.8	56	298.267	19.852
C	M	65	95.3	68.3	72	299.006	19.901
D	M	69	87.2	67.6	77	294.202	19.582
E	M	50	87.2	65.1	75	297.898	19.828
F	F	53	68.4	41.6	61	303.072	20.172
I	F	60	91.1	45.3	50	302.333	20.123
L	M	48	90.5	70.8	78	300.854	20.024
M	M	44	86.4	61.4	71	300.485	20.000
N	F	69	70.2	39.5	56	299.376	19.926
Q	F	54	90.6	51.6	57	300.115	19.975

BW is Body Weight, FFM is Fat-Free Mass, $Dose_{AA+i}$ is the injected dose of AA+i (at time t=0 minutes. The subscript AA denotes the amino acid (Phe or Tyr) and subscripts +6 and +4 represent the component of the tracer (L-[ring-13C6] and L-[ring-2H4], respectively).

hand was placed in a thermostatically controlled hot box (internal temperature: 55°C), a technique to mimic direct arterial sampling [1]. Before i.v. administration of the isotopes, a venous blood sample was collected to measure baseline tracer enrichments. All isotopes are from Cambridge Isotope Laboratories (Woburn, MA, USA). Arterialized-venous blood was sampled for 2 hours for analysis of tracer enrichments and concentrations of amino acids. Samples were collected at the timepoints t=5, 10, 15, 20, 28, 40, 50, 58, 90, 120 minutes.

2.1.3 Biochemical Analysis

Arterialized-venous blood was put in Li-heparinized tubes (Becton Dickinson Vacutainer system, Franklin Lakes, New Jersey, USA), immediately put on ice to minimize enzymatic reactions, and centrifuged (4°C, 3120 x g for 5 min) to obtain plasma. 250 μl Of plasma was put in 50% sulfosalicylic acid (SSA) for deproteinization. Samples were instantly frozen and stored at -80°C until further analysis. Tracer enrichments [tracer:tracee ratio (TTR)] and plasma amino acid concentrations were analyzed by LC-MS/MS by isotope dilution [24]. All samples were analyzed in one batch.
The tracer-tracee ratio as described by Buckley [6] and Cobelli [12, 13] was used for the (non) compartmental modeling.

2.2 Non Compartmental Analysis

SAAM II (Version 1.2.1, SAAM Institute, University of Washington) was used to perform the multiexponential fit of the three measured TTR decays (L-[ring-$^{2}H_4$]-Tyr, L-[ring-$^{13}C_6$]-Phe and L-[ring-$^{13}C_6$]-Tyr). Measurement errors were assumed to be Gaussian i.i.d. with zero mean and a constant fractional SD of 0.01. The precision of the estimates was determined from the inverse of Fisher information matrix.

2.2.1 Optimal Order Selection

The first step of the non-compartmental analysis is the selection of the optimal order of the multiexponential fit of each TTR curve (L-[ring-$^{2}H_4$]-Tyr, L-[ring-$^{13}C_6$]-Phe and L-[ring-$^{13}C_6$]-Tyr) to be used in the individual estimates. To do this, the mean subject (data average of each TTR curve) was chosen as representative of the study population. Single pulse injected L-[ring-$^{13}C_6$]-Phe ($y_a(t)$) and L-[ring-$^{2}H_4$]-Tyr ($y_b(t)$) mean subject TTR curves were fitted by means of the 1-exponential ((2.1) and (2.4), respectively), 2-exponential ((2.2) and (2.5), respectively) and 3-exponential ((2.3) and (2.6), respectively) data models:

$$y_a(t) = A_1 e^{-a_1 t} \tag{2.1}$$

$$y_a(t) = A_1 e^{-a_1 t} + A_2 e^{-a_2 t} \tag{2.2}$$

$$y_a(t) = A_1 e^{-a_1 t} + A_2 e^{-a_2 t} + A_3 e^{-a_3 t} \tag{2.3}$$

$$y_b(t) = B_1 e^{-b_1 t} \tag{2.4}$$

$$y_b(t) = B_1 e^{-b_1 t} + B_2 e^{-b_2 t} \tag{2.5}$$

$$y_b(t) = B_1 e^{-b_1 t} + B_2 e^{-b_2 t} + B_3 e^{-b_3 t} \tag{2.6}$$

Metabolite L-[ring-$^{13}C_6$]-Tyr ($y_c(t)$) appearance and decay in the mean subject's TTR curve was fitted by means of the 2-exponential (2.7) and 3-exponential (2.8) data models:

$$y_c(t) = C_1 e^{-c_1 t} + C_2 e^{-c_2 t} \tag{2.7}$$

$$y_c(t) = C_1 e^{-c_1 t} + C_2 e^{-c_2 t} + C_3 e^{-c_3 t} \tag{2.8}$$

The constraints $C_1 + C_2 = 0$ and $C_1 + C_2 + C_3 = 0$ were used in (2.7) and (2.8), respectively in order to describe the curve properly. Goodness of

the fit (weighted residuals pattern), precision of the estimates, AIC (Akaike Information Criterion) were the ingredients used to assess the optimal order of each TTR curve for the individual non-compartmental analysis.

2.2.2 Individual Analysis

As the optimal order selection results suggests (Section 3.1.1), single pulse injected L-[ring-$^{13}C_6$]-Phe ($y_a(t)$) and L-[ring-$^{2}H_4$]-Tyr ($y_b(t)$) individual TTR decay curves were fitted by means of the 2-exponential data model ((2.2) and (2.5), respectively), while metabolite L-[ring-$^{13}C_6$]-Tyr ($y_c(t)$) appearance and decay in the individual TTR curves were fitted by means of the 3-exponential data model (2.8).
The estimation of the unknown parameters (A_1, A_2, a_1, a_2, B_1, B_2, b_1, b_2, C_1, C_2, C_3, c_1, c_2, c_3) was performed both by considering all data points and by discarding samples at t=5 and 10 minutes in Tyr TTR curves, in order to verify the impact of such assumption (as it was made necessary by the compartmental analysis). The unknown parameters were used to compute areas under the curve (AUC_{AA+i}) as described by the following formulae [36]:

$$AUC_{Phe+6} = \frac{A_1}{a_1} + \frac{A_2}{a_2} \tag{2.9}$$

$$AUC_{Tyr+4} = \frac{B_1}{b_1} + \frac{B_2}{b_2} \tag{2.10}$$

$$AUC_{Tyr+6} = \frac{C_1}{c_1} + \frac{C_2}{c_2} + \frac{C_3}{c_3} \tag{2.11}$$

The rates of appearance ($R_{a,Phe}$) of every amino acid in plasma and the conversion rate of Phe to Tyr ($Phe \rightarrow Tyr$) were then obtained according to the following equations [36]:

$$R_{a,Phe} = \frac{Dose_{Phe+6}}{AUC_{Phe+6}} \tag{2.12}$$

$$R_{a,Tyr} = \frac{Dose_{Tyr+4}}{AUC_{Tyr+4}} \tag{2.13}$$

$$Phe \rightarrow Tyr = R_{a,Tyr} \frac{AUC_{Tyr+6}}{AUC_{Phe+6}} \tag{2.14}$$

$Dose_{AA+i}$ denotes the amount of the bolus of tracer administered at time t=0 min, the subscript AA denotes the amino acid (Phe or Tyr) and subscripts +6 and +4 represent the component of the tracer (L-[ring-$^{13}C_6$] and L-[ring-$^{2}H_4$], respectively).

2.3 Compartmental Analysis

The bolus of L-[ring-$^{2}H_4$]-Tyr and L-[ring-$^{13}C_6$]-Phe isotopes enables the measurement of the Tyr and Phe kinetics. Furthermore, the portion of the L-[ring-$^{13}C_6$]-Phe isotope that is converted into L-[ring-$^{13}C_6$]-Tyr is reflected by the tracer-tracee ratio (TTR) of L-[ring-$^{13}C_6$]-Tyr detected in plasma. Using the plasma TTRs of Phe and Tyr, two compartmental models were developed to analyze the tracer and tracee data.
The first step in model identification is the a priori identifiability analysis of the model [9], which determines whether the model with its input-output experimental configuration has a unique or multiple solutions for its parameters given the ideal condition of noise-free data and error-free model structure. This *a priori* identifiabilty analysis was done by using the program DAISY (Version 1.9, University of Cagliari and University of Padova) [3] for both models. The numerical identification of the models was performed by using the modeling software SAAM II (Version 2.2.1, SAAM Institute, University of Washington) [2]. Measurement errors were assumed to be Gaussian i.i.d. with zero mean and a constant fractional SD equal to 0.01. The precision of the parameters estimates was determined from the inverse of the Fisher information matrix.
Tyr samples at t=5 and 10 minutes were not considered, since they were systematically underestimated. It is likely that the first two samples of the Tyr curves might have been affected from a mixing pool issue [21, 27]. Further details are presented in Chapter 4.

2.3.1 The Four Compartments Model (Model 1)

The previously described non-compartmental analysis suggests that a simple compartmental model made up by four compartments, two compartments for each amino acid, could describe data with the same reliability [36].
The Model is shown in Figure 2.1. Both compartments 1 and 2 represent Phe: Compartment 1 is the pool in which Phe is sampled and represents plasma and rapidly equilibrating tissues, while Compartment 2 represents Phe in tissues that are exchanging with Compartment 1 with a slower kinetics. Irreversible losses from both compartments 1 and 2 represent protein synthesis. Similarly to Phe, compartments 3 and 4 represent Tyr. Irreversible losses from both compartments 3 and 4 represent protein synthesis and oxidation. The link between compartments 1 and 3 represents the hydroxylation flux of Phe into its metabolite Tyr which takes place in fast exchanging tissues [26]. L-[ring-$^{13}C_6$]-Phe and L-[ring-$^{2}H_4$]-Tyr were introduced into compartments 1 and 3 respectively and the corresponding tracer-tracee ratio data was measured in plasma, while a portion of the L-[ring-$^{13}C_6$]-Phe isotope is converted into L-[ring-$^{13}C_6$]-Tyr and its tracer-tracee ratio data was also measured in plasma (Compartment 3 in the model).

The tracer model is described by the following equations:

- Tracer 1 (L-[ring-$^{13}C_6$]):

$$\frac{dq_1^{+6}}{dt}(t) = -(k_{01} + k_{21} + k_{31})q_1^{+6}(t) + k_{12}q_2^{+6}(t) + u_1 \tag{2.15}$$
$$\frac{dq_2^{+6}}{dt}(t) = k_{21}q_1^{+6}(t) - (k_{02} + k_{12})q_2^{+6}(t) \tag{2.16}$$
$$\frac{dq_3^{+6}}{dt}(t) = k_{31}q_1^{+6}(t) - (k_{03} + k_{43})q_3^{+6}(t) + k_{34}q_4^{+6}(t) \tag{2.17}$$
$$\frac{dq_4^{+6}}{dt}(t) = k_{43}q_3^{+6}(t) - (k_{04} + k_{34})q_4^{+6}(t) \tag{2.18}$$

- Tracer 2 (L-[ring-$^{2}H_4$]):

$$\frac{dq_3^{+4}}{dt}(t) = k_{31}q_1^{+4}(t) - (k_{03} + k_{43})q_3^{+4}(t) + k_{34}q_4^{+4}(t) + u_2 \tag{2.19}$$
$$\frac{dq_4^{+4}}{dt}(t) = k_{43}q_3^{+4}(t) - (k_{04} + k_{34})q_4^{+4}(t) \tag{2.20}$$

Where q_i is tracer mass of compartment i ($i = 1, 2, 3, 4$), with the initial condition $q_i(0) = 0$; q_i is the sum of the labeled (artificially elevated in the tracer) and the unlabeled (predominating in the tracee) species due to the exogenously introduced material. The superscripts $+6$ and $+4$ denote the components of the tracers L-[ring-$^{13}C_6$] and L-[ring-$^{2}H_4$], respectively. u_1 and u_2 are the pulse tracer inputs of Phe and Tyr, respectively. The three measurement equations are:

$$TTR_1(t) = \frac{q_1^{+6}(t)}{Q_1} \tag{2.21}$$

$$TTR_2(t) = \frac{q_3^{+6}(t)}{Q_3} \tag{2.22}$$

$$TTR_3(t) = \frac{q_3^{+4}(t)}{Q_3} \tag{2.23}$$

Q_1 and Q_3 are the tracee masses, i.e., the sum of the labeled and unlabeled species present in the naturally occurring material of compartments 1 and 3, respectively.
The tracee system is assumed to be in steady state during the study period. Therefore, it is described by the following equations:

$$0 = -(k_{01} + k_{21} + k_{31})Q_1 + k_{12}Q_2 + U_1 \tag{2.24}$$
$$0 = k_{21}Q_1 - (k_{02} + k_{12})Q_2 + U_2 \tag{2.25}$$
$$0 = k_{31}Q_1 - (k_{03} + k_{43})Q_3 + k_{34}Q_4 + U_3 \tag{2.26}$$
$$0 = k_{43}Q_3 - (k_{04} + k_{34})Q_4 + U_4 \tag{2.27}$$

Where Q_i are the tracee masses and U_i are the endogenous productions (U_1, U_2 and U_3, U_4 of Phe and Tyr, respectively) coming from protein catabolism. Q_1, Q_3 and the k_{ij} are estimated from the tracer model. The products $k_{ij}Q_j$ are the fluxes F_{ij}. This way, the disposals F_{01}, F_{02} represent Phe going into protein anabolism, while F_{03} and F_{04} represent Tyr either being included in proteins or being oxidized.

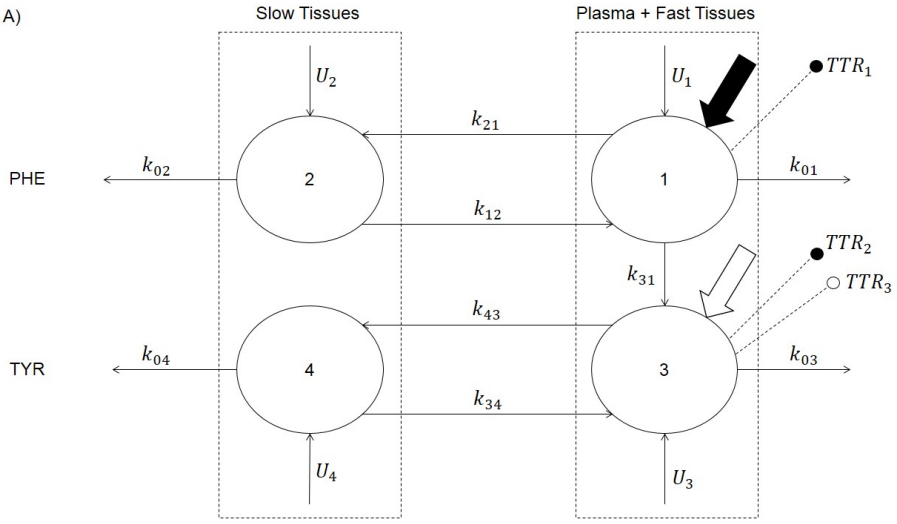

Figure 2.1: The four compartments model of Phe-Tyr kinetics (Model 1)

The circles indicate compartments representing kinetically distinct pools of Phenylalanine and Tyrosine and the arrows between them the intercompartmental fluxes. k_{ij} (per minute) are the transfer rate constants of flux from compartment j to compartment i. Large arrows denote Phe (solid arrow) and Tyr (open arrow) tracer inputs. TTR_i measurements are indicated by dashed lines ending with solid (from Phe tracer input) or open (from Tyr tracer input) circle, respectively.

Model Identification

The *a priori* identifiability analysis of Model 1 revealed that the model is non-uniquely identifiable, meaning that there are multiple solutions for some

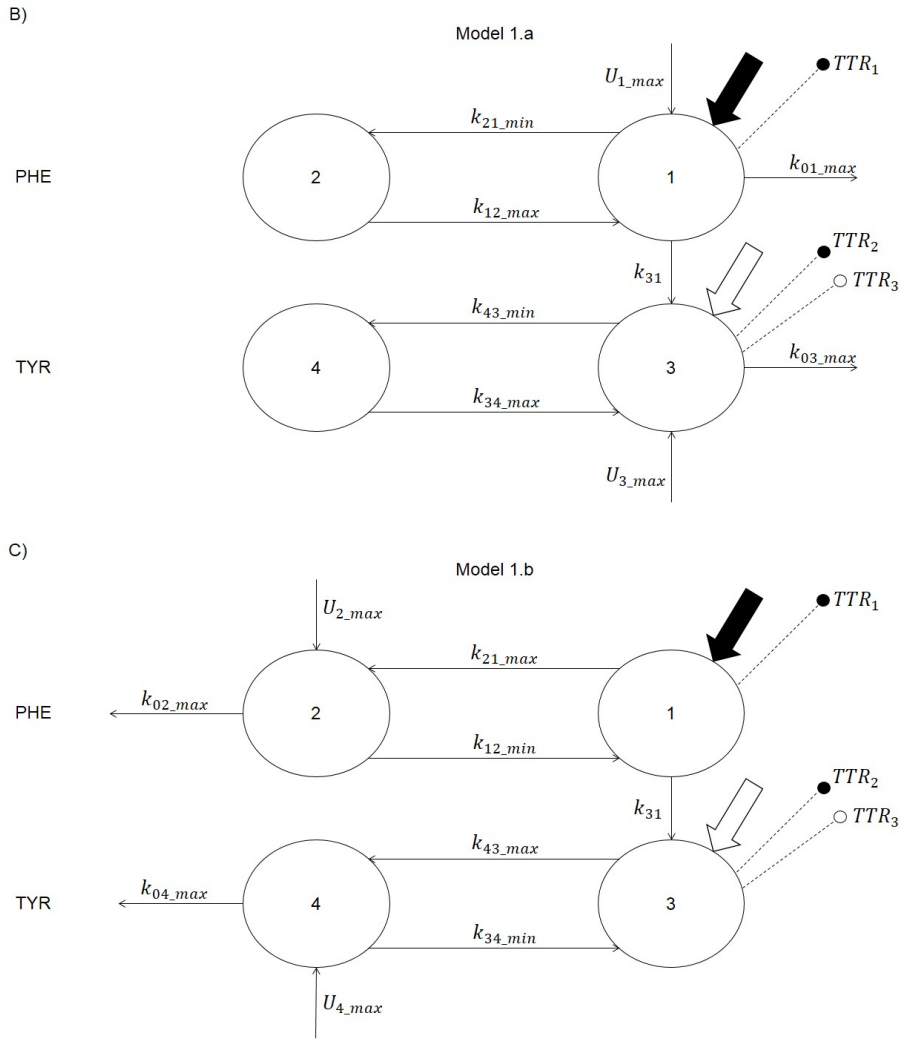

Figure 2.2: Interval identification strategy (Model 1)

Unidentifiable parameters of the model shown in Figure 2.1, Panel A are quantified in terms of upper and lower bounds of intervals of admissible values, by use of the two submodels shown in panels B and C.

of the unknown parameters. In particular, k_{31}, Q_1 and Q_3 are uniquely identifiable, while all the remaining parameters (k_{12}, k_{21}, etc.) are not uniquely identifiable. Indeed, this is due to the fact that each amino acid has one input and two possible exits from the system: the main issue here is that it is not trivial to find a relationship between the irreversible losses from the pools of each amino acid. As regards the tracee parameters, U_1, U_2, U_3, U_4 and Q_2, Q_4 cannot be solved from eq. (2.24), (2.25), (2.26), (2.27), since the

number of unknowns (6) exceeds the number of equations (4). Therefore, the model described in Figure 1 was used to find upper and lower bounds for its parameters. To achieve this, estimation from interval identifiable models [19, 10] was used. The adopted identification strategy is depicted in Figure 2.2 showing how the non-uniquely identifiable tracer/tracee model is split into two uniquely identifiable submodels: Model 1.a and Model 1.b. The first submodel (Model 1.a), by setting $k_{02} = k_{04} = U_2 = U_4 = 0$ provides values for the uniquely identifiable parameters (Q_1, Q_3 and k_{31}), upper bounds for k_{12}, k_{34}, k_{01}, k_{03}, U_1, U_3, F_{01}, F_{03} and lower bounds for k_{21}, k_{43}, k_{02}, k_{04}, Q_2, Q_4, F_{21}, F_{12}, F_{43}, F_{34}, F_{02}, F_{04}. The second submodel (Model 1.b), by setting $k_{01} = k_{03} = U_1 = U_3 = 0$ provides values for the uniquely identifiable parameters (Q_1, Q_3 and k_{31}), upper bounds for k_{21}, k_{43}, k_{02}, k_{04}, Q_2, Q_4, F_{21}, F_{12}, F_{43}, F_{34}, U_2, U_4, F_{02}, F_{04} and the lower bounds for k_{12}, k_{34}, k_{01}, k_{03}, U_1, U_3, F_{01}, F_{03}. The hydroxylation flux F_{31} has a unique solution, common to both submodels because it is expressed in terms of Q_1 and k_{31} which are uniquely identifiable. Each submodel was numerically identified in every subject by using nonlinear least-squares to fit the three TTR curves using the program SAAM II [2].

2.3.2 The Six Compartments Model (Model 2)

The previously described Model provides an useful insight in the metabolism of Phe-Tyr kinetics in the postabsorptive state, along with accurate measurements for the hydroxylation flux. Nevertheless, the model is non-uniquely identifiable and only allows possible intervals of estimation for most of the unknown parameters [19, 10]. In order to overcome this identifiability issue, the development of a more complex compartmental model was necessary. Later, it was possible to validate some of the structural assumptions made in the design phase by using the model to simulate a continuous infusion experiment previously done on pigs (Section 4.2.6).

The Model is shown in Figure 2.3. Compartments 1, 2 and 5 represent Phe: Compartment 1 is the pool in which Phe is sampled and represents extracellular (EC) fluid; Compartment 2 represents intracellular (IC) Phe in tissues that are exchanging with Compartment 1 with a slow kinetics; Compartment 5 represents intracellular (IC) Phe in tissues that are exchanging with Compartment 1 with a fast kinetics and are responsible for the conversion to Tyr. The irreversible loss from Compartment 2 represents protein synthesis. Similarly to Phe, compartments 3, 4 and 6 represent Tyr. The irreversible loss from compartment 4 represents protein synthesis and oxidation. The link between compartments 5 and 6 represents the hydroxylation flux of Phe into its metabolite Tyr, which takes place at the intracellular level in fast exchanging tissues [26]. Similarly to Model 1, L-[ring-$^{13}C_6$]-Phe and L-[ring-$^{2}H_4$]-Tyr were introduced into Compartment 1 and 3 respectively and the corresponding tracer-tracee ratio data was measured in plasma, while a

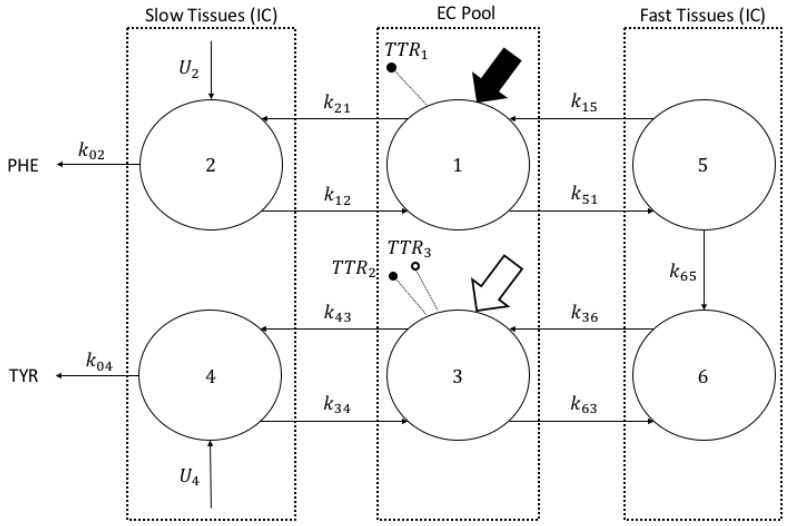

Figure 2.3: The six compartments model of Phe-Tyr kinetics (Model 2)

The notation used is the same of Figure 2.1

portion of the L-[ring-$^{13}C_6$]-Phe isotope is converted into L-[ring-$^{13}C_6$]-Tyr and its tracer-tracee ratio data was also measured in plasma (Compartment 3 in the model).
The tracer model is described by the following equations:

- Tracer 1 (L-[ring-$^{13}C_6$]):

$$\frac{dq_1^{+6}}{dt}(t) = -(k_{21} + k_{51})q_1^{+6}(t) + k_{12}q_2^{+6}(t) + k_{15}q_5^{+6}(t) + u_1 \tag{2.28}$$
$$\frac{dq_2^{+6}}{dt}(t) = k_{21}q_1^{+6}(t) - (k_{02} + k_{12})q_2^{+6}(t) \tag{2.29}$$
$$\frac{dq_3^{+6}}{dt}(t) = -(k_{43} + k_{63})q_3^{+6}(t) + k_{34}q_4^{+6}(t) + k_{36}q_6^{+6}(t) \tag{2.30}$$
$$\frac{dq_4^{+6}}{dt}(t) = k_{43}q_3^{+6}(t) - (k_{04} + k_{34})q_4^{+6}(t) \tag{2.31}$$
$$\frac{dq_5^{+6}}{dt}(t) = k_{51}q_1^{+6}(t) - (k_{15} + k_{65})q_5^{+6}(t) \tag{2.32}$$
$$\frac{dq_6^{+6}}{dt}(t) = k_{63}q_3^{+6}(t) + k_{65}q_5^{+6}(t) - k_{36}q_6^{+6}(t) \tag{2.33}$$

- Tracer 2 (L-[ring-$^{2}H_4$]):

$$\frac{dq_3^{+4}}{dt}(t) = -(k_{43} + k_{63})q_3^{+4}(t) + k_{34}q_4^{+4}(t) + k_{36}q_6^{+4}(t) + u_2 \tag{2.34}$$

$$\frac{dq_4^{+4}}{dt}(t) = k_{43}q_3^{+4}(t) - (k_{04} + k_{34})q_4^{+4}(t) \tag{2.35}$$

$$\frac{dq_6^{+4}}{dt}(t) = k_{63}q_3^{+4}(t) + k_{65}q_5^{+4}(t) - k_{36}q_6^{+4}(t) \tag{2.36}$$

Where the notation follows the same convention used in Model 1. Similarly, the three measurement equations are (2.21), (2.22), (2.23) and the tracee system is assumed to be in steady state during the study period. Therefore, it is described by the following equations:

$$0 = -(k_{21} + k_{51})Q_1 + k_{12}Q_2 + k_{15}Q_5 \tag{2.37}$$

$$0 = k_{21}Q_1 - (k_{02} + k_{12})Q_2 + U_2 \tag{2.38}$$

$$0 = -(k_{43} + k_{63})Q_3 + k_{34}Q_4 + k_{36}Q_6 \tag{2.39}$$

$$0 = k_{43}Q_3 - (k_{04} + k_{34})Q_4 + U_4 \tag{2.40}$$

$$0 = k_{51}Q_1 - (k_{15} + k_{65})Q_5 \tag{2.41}$$

$$0 = k_{63}Q_3 + k_{65}Q_5 - k_{36}Q_6 \tag{2.42}$$

Where Q_i are the tracee masses and U_i are the endogenous productions (U_2 and U_4 of Phe and Tyr, respectively) coming from protein catabolism. k_{ij} are estimated from the tracer model, whereas Q_1 and Q_3 are estimated *a priori* from plasma concentrations of Phe and Tyr (see Model Identification section for further details). The products $k_{ij}Q_j$ are the fluxes F_{ij}. This way, the disposal F_{02} represents Phe going into protein anabolism, while F_{04} represents Tyr either being included in proteins or being oxidized.

Model Identification

The *a priori* identifiability analysis of Model 2 revealed that the model is uniquely identifiable, meaning that there is one unique solution for every unknown parameter. Nevertheless, since samples at t=5 and 10 minutes of Tyr curves were not considered [21, 27] and the model structure accounts for 2 more compartments than Model 1, estimating the accessible pool sizes Q_1 and Q_3 directly from the dataset is quite troublesome. Therefore, their dimensions were calculated *a priori* from the fat-free mass (FFM) and plasma concentrations of Phe and Tyr of every subject, according to the following equations:

$$TBW = 0.73\ FFM \tag{2.43}$$

Table 2.2: *A priori* estimation of Q_1 and Q_3

Subject	FFM (kg)	TBW (L)	EC_{vol} (L)	$[Phe]_{EC}$ (μM)	$[Tyr]_{EC}$ (μM)	Q_1 (μmol)	Q_3 (μmol)
A	65.1	47.5	15.8	44.5	46.4	705	735
B	50.8	37.1	12.4	49.9	42.7	617	527
C	68.3	49.9	16.6	54.0	63.6	898	1057
D	67.6	49.4	16.5	41.6	38.2	685	628
E	65.1	47.5	15.8	38.4	42.8	609	677
F	41.6	30.4	10.1	29.9	33.7	303	341
I	45.3	33.0	11.0	41.7	40.7	459	449
L	70.7	51.6	17.2	36.8	38.2	634	657
M	61.4	44.8	14.9	35.6	33.6	532	502
N	39.5	28.8	9.6	42.3	43.6	407	418
Q	51.6	37.7	12.6	36.5	42.1	458	528
Mean	57.0	41.6	13.9	41.0	42.3	573	593
SEM	11.5	8.4	2.8	6.8	8.1	165	195

$$EC_{vol} = \frac{1}{3}\, TBW \tag{2.44}$$

$$Q_1 = [Phe]_{EC} EC_{vol} \tag{2.45}$$

$$Q_3 = [Tyr]_{EC} EC_{vol} \tag{2.46}$$

TBW stands for Total Body Water and EC_{vol} for the total extracellular (EC) volume of the body. $[Phe]_{EC}$ and $[Tyr]_{EC}$ are the extracellular concentrations of Phe and Tyr, respectively. It is assumed that $[Phe]_{plasma} = [Phe]_{EC}$ and $[Tyr]_{plasma} = [Tyr]_{EC}$. The computed values for every subject are reported in Table 2.2. The *a priori* calculated values of Q_1 a Q_3 were therefore used in SAAM II as fixed variables.

Because of the limited number of data points available in the first phase of the experiment (given the already mentioned Tyr mixing issue [21, 27]), *maximum likelihood* (ML) estimation of some of the unknown parameters (k_{15}, k_{36}, k_{51} and k_{63}) was not possible. For this reason, *maximum a priori* (MAP) estimation was used for such kinetic parameters, by means of the following a priori information:

$$k_{15} : \mu = 1.016, \sigma = 0.102 \tag{2.47}$$

$$k_{36} : \mu = 1.016, \sigma = 0.102 \tag{2.48}$$

$$k_{51} : \mu = 0.031, \sigma = 0.003 \tag{2.49}$$

$$k_{63} : \mu = 0.017, \sigma = 0.002 \tag{2.50}$$

This *a priori* information was gleaned based on the assumption that EC (compartments 1 and 3) and IC pools for hydroxylation (compartments 5 and 6) mix very rapidly [35, 23] and was later validated by using the model to perform a continuous infusion experiment previously done on pigs (Section 4.2.6).

Chapter 3

Results

3.1 Non Compartmental Analysis

3.1.1 Optimal Order selection

The non-compartmental data models used on the mean subject allow for some observations. In general, the two-exponential and the three-exponential models provide a good fit for the L-[ring-$^{13}C_6$]-Phe and L-[ring-$^{2}H_4$]-Tyr TTR curves, while the one-exponential model is not able to fit the data properly, as shown in Figure 3.1. In particular, the mean weighted residuals' patterns (defined for a given time point as the difference between the datum and the model prediction normalized by the SD of the datum) confirmed by visual inspection the goodness of the fit. Nevertheless, for these two TTR curves the two-exponential data model shows a higher precision of the estimates compared to the three-exponential one, together with a lower AIC (tables 3.1 and 3.2). Therefore, it is possible to conclude that a two-exponential data model is the optimal order for the non-compartmental fitting of the L-[ring-$^{13}C_6$]-Phe and L-[ring-$^{2}H_4$]-Tyr TTR curves. As far as the L-[ring-$^{13}C_6$]-Tyr TTR curve is concerned, the three-exponential model provides a good fit of the mean subject data, whereas the two-exponential model is unable to do the same (Figure 3.1). It is therefore possible to conclude that a three-exponential data model is the optimal order for the non-compartmental fitting of the L-[ring-$^{13}C_6$]-Tyr TTR curve.

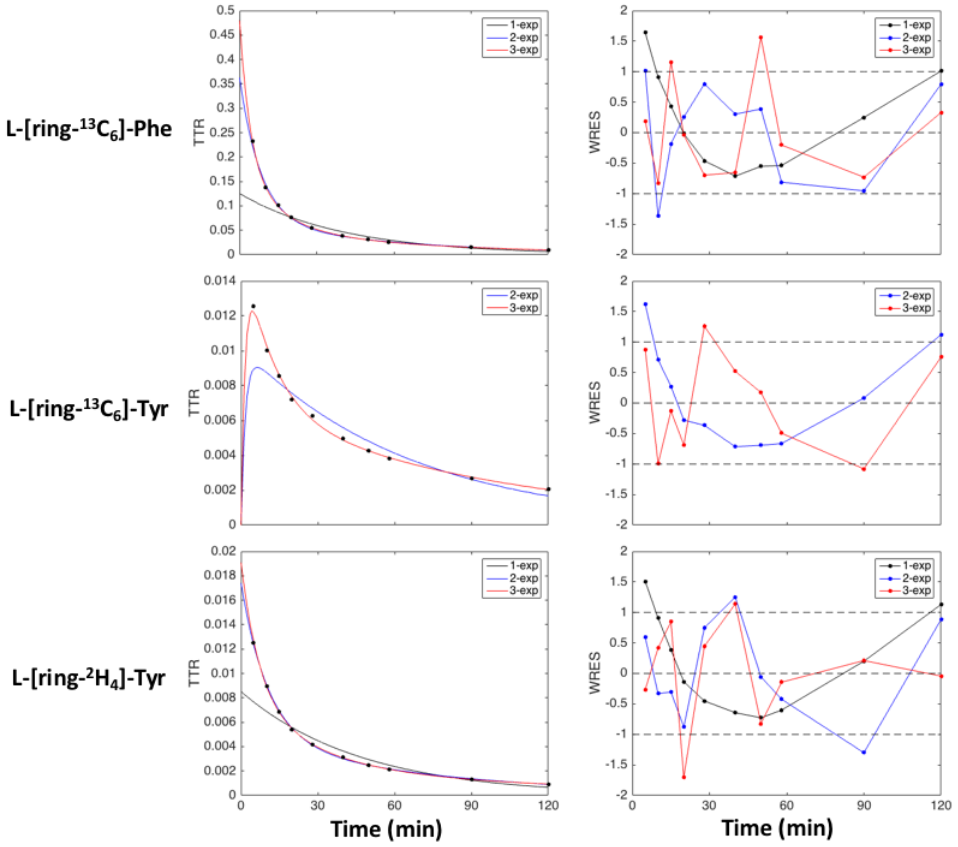

Figure 3.1: Ability of the non-compartmental data models to fit mean subject data (optimal order selection)

Average Data (solid dots) vs. model fit (continuous line) in left panels, weighted residuals in right panels. Weighted residuals are defined as the difference between data and model prediction normalized to SD of data. Continuous black line represents one-exponential, continuous blue line represents 2-exponential and continuous red line represents three-exponential data models.

Table 3.1: Mean Subject L-[ring-$^{13}C_6$]-Phe (y_a) multiexponential parameters and AIC

	A_1	A_2	A_3	a_1	a_2	a_3	AIC
1-exp	0.125 (20%)			0.025 (15%)			8.10
2-exp	0.295 (8%)	0.068 (6%)		0.121 (7%)	0.016 (4%)		10.10
3-exp	0.288 (12%)	0.138 (24%)	0.054 (11%)	0.243 (22%)	0.071 (18%)	0.014 (7%)	12.10

A_i are adimensional, a_i are min^{-1}. The number between brackets indicates the precision of the estimate, defined as CV% = 100 SD($p_{i,est}$)/$p_{i,est}$, where CV is the coefficient of variation and SD is the standard deviation.

Table 3.2: Mean Subject L-[ring-$^{2}H_4$]-Tyr (y_b) multiexponential parameters and AIC

	B_1	B_2	B_3	b_1	b_2	b_3	AIC
1-exp	0.008 (15%)			0.021 (14%)			8.10
2-exp	0.013 (5%)	0.005 (6%)		0.093 (7%)	0.014 (5%)		10.10
3-exp	0.011 (9%)	0.006 (10%)	0.002 (67%)	0.138 (15%)	0.034 (35%)	0.007 (57%)	12.10

B_i are adimensional, b_i are min^{-1}. The number between brackets indicates the precision of the estimate, defined as CV% = 100 SD($p_{i,est}$)/$p_{i,est}$, where CV is the coefficient of variation and SD is the standard deviation.

Table 3.3: Mean Subject L-[ring-$^{13}C_6$]-Tyr (y_c) multiexponential parameters and AIC

	C_2	C_3	c_1	c_2	c_3	AIC
2-exp	0.010 (10%)		0.599 (59%)	0.015 (12%)		10.10
3-exp	0.010 (9%)	0.007 (7%)	0.629 (10%)	0.086 (14%)	0.010 (7%)	12.10

C_i are adimensional, c_i are min^{-1}. The number between brackets indicates the precision of the estimate, defined as CV% = 100 SD($p_{i,est}$)/$p_{i,est}$, where CV is the coefficient of variation and SD is the standard deviation.

3.1.2 Individual Analysis

The non-compartmental data model used provides a good fit of experimental data, shown in figures 3.2 (complete dataset) and 3.3 (Tyr samples at t=5 and 10 minutes discarded). In particular, the mean weighted residuals' patterns confirmed by visual inspection the goodness of the fit.
The population averages of every parameter are reported in Table 3.4. The single subject estimates are reported in tables 3.5 (L-[ring-$^{13}C_6$]-Phe), 3.6 (L-[ring-$^{2}H_4$]-Tyr and L-[ring-$^{13}C_6$]-Tyr, complete dataset) and 3.7 (L-[ring-$^{2}H_4$]-Tyr and L-[ring-$^{13}C_6$]-Tyr, samples at t=5 and 10 minutes discarded). When all data points were considered, all parameters were estimated with good precision, as all CV%'s are below 50% (except from Subject N's C_2, whose CV% is 72%). When samples at t=5 and 10 minutes in the Tyr TTR curves were not considered, the precision of the estimates of some of the parameters was not optimal (as the maximum CV% is 104% and 8 parameters have a CV% above 50%), due to the limited number of data points available for the estimation. Individual gleaned fluxes are reported in tables 3.8 (complete dataset) and 3.9 (Tyr samples at t=5 and 10 minutes discarded).

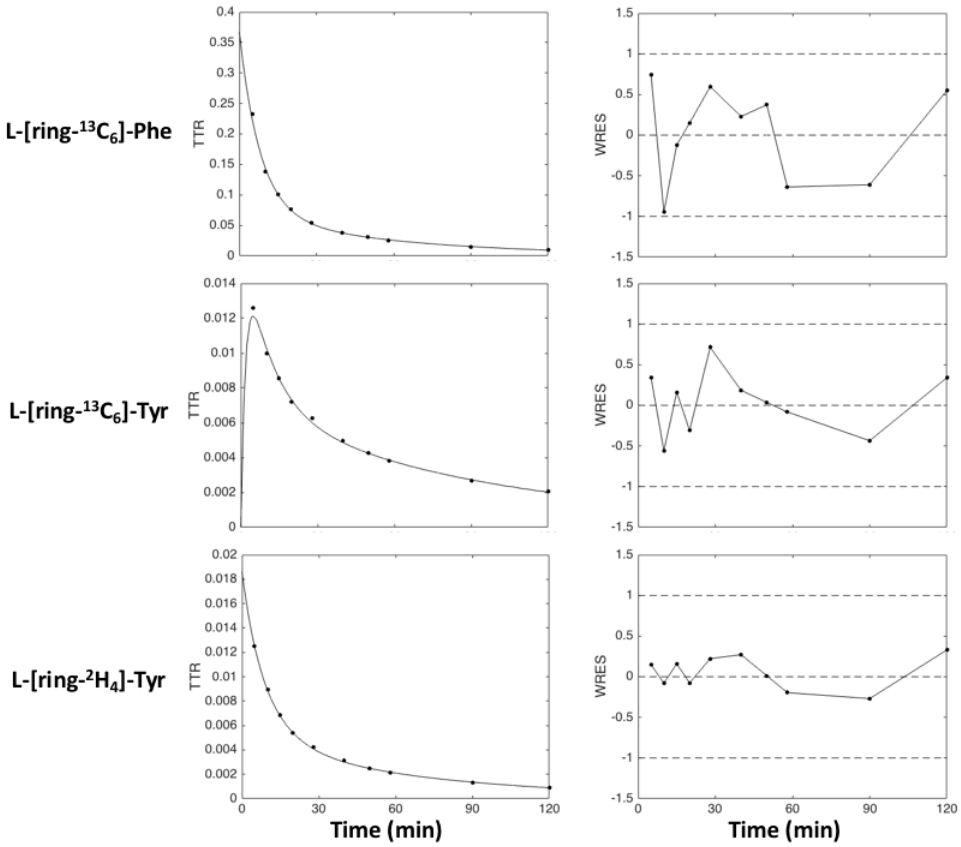

Figure 3.2: Ability of non-compartmental data models to fit data (complete dataset)

Average Data (solid dots) vs. Average model fit (continuous line) in left panels, average weighted residuals in right panels.

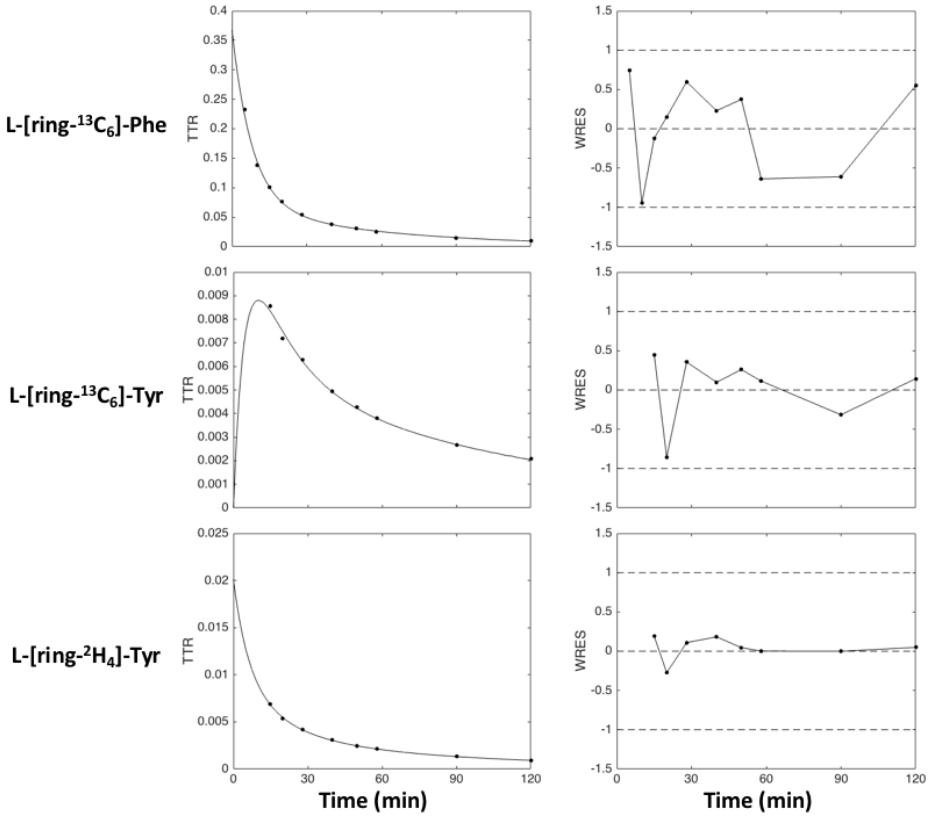

Figure 3.3: Ability of non-compartmental data models to fit data (Tyr samples at t=5 and 10 minutes discarded)

Average Data (solid dots) vs. Average model fit (continuous line) in left panels, average weighted residuals in right panels.

Table 3.4: Average non-compartmental multiexponential parameters, AUCs and non-compartmental fluxes

Variable	**Unit**	**Complete Dataset**	**Partial Dataset**
A_1	adimensional	0.299 ± 0.107	
A_2	adimensional	0.068 ± 0.025	
a_1	min^{-1}	0.119 ± 0.016	
a_2	min^{-1}	0.016 ± 0.002	
B_1	adimensional	0.014 ± 0.006	0.017 ± 0.011
B_2	adimensional	0.005 ± 0.002	0.003 ± 0.001
b_1	min^{-1}	0.101 ± 0.038	0.090 ± 0.055
b_2	min^{-1}	0.014 ± 0.001	0.011 ± 0.002
C_2	adimensional	0.013 ± 0.006	0.014 ± 0.007
C_3	adimensional	0.007 ± 0.002	0.006 ± 0.001
c_1	min^{-1}	0.519 ± 0.066	0.204 ± 0.019
c_2	min^{-1}	0.129 ± 0.072	0.081 ± 0.034
c_3	min^{-1}	0.010 ± 0.002	0.009 ± 0.001
AUC_{Phe+6}	min	6.582 ± 1.670	
AUC_{Tyr+4}	min	0.477 ± 0.158	0.501 ± 0.140
AUC_{Tyr+6}	min	0.769 ± 0.190	0.759 ± 0.209
$R_{a,Phe}$	μmol·FFM kg^{-1}·h^{-1}	50.4 ± 4.9	
$R_{a,Tyr}$	μmol·FFM kg^{-1}·h^{-1}	47.8 ± 9.0	44.5 ± 5.7
$Phe \rightarrow Tyr$	μmol·FFM kg^{-1}·h^{-1}	5.7 ± 1.5	5.2 ± 1.3

Values are expressed as Mean ± SEM. The **Partial Dataset** column represents the condition in which samples at t=5 and 10 minutes were not considered in Tyr TTR curves for the estimation. C_1 is not reported, being $C_1 = -(C_2 + C_3)$.

Table 3.5: Individual L-[ring-$^{13}C_6$]-Phe (y_a) multiexponential parameters and AUCs

Subject		A_1	A_2	a_1	a_2	AUC_{Phe+6}
A	Value	0.255	0.050	0.106	0.014	5.884
	CV%	10	11	10	9	2
B	Value	0.185	0.069	0.099	0.013	7.005
	CV%	6	5	8	5	1
C	Value	0.229	0.039	0.116	0.014	4.665
	CV%	14	13	13	11	4
D	Value	0.278	0.046	0.111	0.016	5.443
	CV%	6	7	6	5	2
E	Value	0.301	0.068	0.135	0.018	5.931
	CV%	14	10	13	6	3
F	Value	0.580	0.113	0.148	0.018	10.079
	CV%	12	7	9	5	3
I	Value	0.252	0.075	0.123	0.017	6.469
	CV%	14	10	14	7	3
L	Value	0.263	0.044	0.120	0.017	4.803
	CV%	13	12	11	8	3
M	Value	0.380	0.056	0.141	0.017	5.975
	CV%	11	8	9	6	3
N	Value	0.238	0.110	0.102	0.017	8.970
	CV%	6	5	8	3	1
Q	Value	0.325	0.079	0.114	0.018	7.179
	CV%	9	8	9	5	2
Mean	Value	0.299	0.068	0.119	0.016	6.582
	CV%	10	9	10	6	2
	SEM	0.107	0.025	0.016	0.002	1.670

Values are in min^{-1} (a_i), adimensional (A_i), min (AUC_{Phe+6}). Precisions of estimated parameters are expressed as CV% = 100 SD($p_{i,est}$)/$p_{i,est}$, where CV is the coefficient of variation and SD is the standard deviation.

Table 3.6: Individual L-[ring-$^2H_4$]-Tyr (y_b) and L-[ring-$^{13}C_6$]-Tyr (y_c) multiexponential parameters and AUCs (complete dataset)

Subj.		B_1	B_2	b_1	b_2	C_2	C_3	c_1	c_2	c_3	AUC_{Tyr+4}	AUC_{Tyr+6}
A	Value	0.008	0.003	0.065	0.013	0.010	0.005	0.491	0.045	0.007	0.367	0.894
	CV%	21	21	28	13	11	32	15	25	40	5	14
B	Value	0.011	0.005	0.066	0.013	0.015	0.007	0.533	0.312	0.010	0.508	0.657
	CV%	16	18	23	12	46	6	16	26	9	4	5
C	Value	0.013	0.002	0.111	0.012	0.010	0.004	0.530	0.097	0.009	0.316	0.569
	CV%	22	21	22	20	21	13	23	23	16	6	7
D	Value	0.014	0.003	0.094	0.015	0.017	0.005	0.336	0.076	0.009	0.357	0.758
	CV%	12	17	15	12	21	27	22	28	36	3	13
E	Value	0.012	0.004	0.088	0.014	0.013	0.009	0.566	0.106	0.013	0.405	0.762
	CV%	11	14	15	10	25	11	22	30	10	3	3
F	Value	0.028	0.010	0.204	0.015	0.014	0.012	0.539	0.108	0.010	0.771	1.257
	CV%	35	9	28	8	31	9	23	35	11	4	5
I	Value	0.006	0.004	0.079	0.014	0.007	0.007	0.503	0.181	0.010	0.386	0.727
	CV%	17	18	33	13	48	6	17	32	8	3	5
L	Value	0.015	0.003	0.085	0.012	0.016	0.006	0.545	0.088	0.014	0.403	0.589
	CV%	12	23	16	20	24	25	23	33	19	4	5
M	Value	0.012	0.003	0.098	0.013	0.026	0.007	0.580	0.109	0.010	0.378	0.839
	CV%	9	10	11	8	19	13	22	18	14	2	5
N	Value	0.014	0.006	0.109	0.011	0.001	0.006	0.552	0.169	0.008	0.664	0.753
	CV%	22	16	28	16	72	3	15	40	5	6	3
Q	Value	0.023	0.008	0.113	0.016	0.010	0.007	0.531	0.123	0.012	0.688	0.653
	CV%	17	13	19	10	28	6	23	24	6	3	3
Mean	Value	0.014	0.005	0.101	0.014	0.013	0.007	0.519	0.129	0.010	0.477	0.769
	CV%	18	16	22	13	31	14	20	28	16	4	6
	SEM	0.006	0.002	0.038	0.001	0.006	0.002	0.066	0.072	0.002	0.158	0.190

Values are in min^{-1} (b_i, c_i), adimensional (B_i, C_i), min (AUC_{AA+i}). Precisions of estimated parameters are expressed as CV% = 100 SD$(p_{i,est})/p_{i,est}$, where CV is the coefficient of variation and SD is the standard deviation.

Table 3.7: Individual L-[ring-$^{2}H_4$]-Tyr (y_b) and L-[ring-$^{13}C_6$]-Tyr (y_c) multiexponential parameters and AUCs (samples at t=5 and 10 minutes discarded)

Subj.		B_1	B_2	b_1	b_2	C_2	C_3	c_1	c_2	c_3	AUC_{Tyr+4}	AUC_{Tyr+6}
A	Value	0.011	0.003	0.065	0.010	0.015	0.006	0.207	0.073	0.009	0.410	0.802
	CV%	31	31	29	27	32	15	14	29	17	8	6
B	Value	0.011	0.003	0.051	0.009	0.020	0.006	0.210	0.144	0.009	0.533	0.675
	CV%	21	47	30	40	77	6	14	25	8	8	4
C	Value	0.042	0.003	0.170	0.013	0.018	0.004	0.211	0.108	0.008	0.449	0.553
	CV%	58	10	21	9	57	12	14	27	17	21	7
D	Value	0.012	0.003	0.092	0.015	0.025	0.006	0.212	0.092	0.010	0.346	0.712
	CV%	17	9	14	6	41	20	14	28	25	3	9
E	Value	0.009	0.003	0.060	0.011	0.011	0.005	0.217	0.045	0.008	0.399	0.787
	CV%	8	21	15	16	15	17	14	18	16	2	5
F	Value	0.009	0.003	0.030	0.008	0.015	0.008	0.149	0.048	0.007	0.758	1.336
	CV%	15	31	19	27	45	24	29	40	26	8	10
I	Value	0.036	0.005	0.198	0.015	0.009	0.007	0.200	0.132	0.010	0.510	0.705
	CV%	74	4	25	3	72	10	15	29	13	18	7
L	Value	0.013	0.002	0.074	0.011	0.013	0.003	0.207	0.045	0.008	0.404	0.594
	CV%	24	32	25	28	16	33	15	19	32	5	8
M	Value	0.009	0.003	0.072	0.012	0.020	0.005	0.220	0.073	0.008	0.367	0.816
	CV%	13	15	16	12	36	18	30	26	20	2	7
N	Value	0.020	0.006	0.140	0.012	0.001	0.006	0.202	0.061	0.008	0.685	0.735
	CV%	66	11	35	12	104	6	14	76	8	9	4
Q	Value	0.012	0.003	0.042	0.009	0.007	0.006	0.213	0.073	0.011	0.653	0.631
	CV%	12	30	15	25	49	16	14	50	15	5	5
Mean	Value	0.017	0.003	0.090	0.011	0.014	0.006	0.204	0.081	0.009	0.501	0.759
	CV%	31	22	22	19	49	16	17	33	18	8	7
	SEM	0.011	0.001	0.055	0.002	0.007	0.001	0.019	0.034	0.001	0.140	0.209

Values are in min^{-1} (b_i, c_i), adimensional (B_i, C_i), min (AUC_{AA+i}). Precisions of estimated parameters are expressed as CV% = 100 SD$(p_{i,est})/p_{i,est}$, where CV is the coefficient of variation and SD is the standard deviation.

Table 3.8: Individual non-compartmental fluxes (complete dataset)

Subject	$R_{a,Phe}$	$R_{a,Tyr}$	$Phe \rightarrow Tyr$
A	47.2	50.3	7.6
B	50.3	46.1	4.3
C	56.3	55.4	6.8
D	48.0	48.7	6.8
E	46.3	45.2	5.8
F	43.3	37.7	4.7
I	62.0	69.1	7.8
L	53.1	42.1	5.2
M	49.2	51.8	7.3
N	50.7	45.6	3.8
Q	48.6	33.8	3.1
Mean	50.4	47.8	5.7
SEM	4.9	9.0	1.5

Values are in μmol·FFM kg^{-1}·h^{-1}.

Table 3.9: Individual non-compartmental fluxes (Tyr samples at t=5 and 10 minutes discarded)

Subject	$R_{a,Phe}$	$R_{a,Tyr}$	$Phe \rightarrow Tyr$
A	47.2	45.0	6.1
B	50.3	43.9	4.2
C	56.3	38.9	4.6
D	48.0	50.3	6.6
E	46.3	45.9	6.1
F	43.3	38.4	5.1
I	62.0	52.3	5.7
L	53.1	42.1	5.2
M	49.2	53.3	7.3
N	50.7	44.2	3.6
Q	48.6	35.6	3.1
Mean	50.4	44.5	5.2
SEM	4.9	5.7	1.3

Values are in μmol·FFM kg^{-1}·h^{-1}.

3.2 Compartmental Analysis

3.2.1 The Four Compartments Model (Model 1)

The submodels provide a good fit of experimental data, shown in Figure 3.4. In particular, the mean weighted residuals' patterns confirmed by visual inspection the goodness of the fit.
The population average upper and lower bounds of every parameter are reported in Table 3.10, while the individual values are reported for every submodel in tables 3.11, 3.13 (Model 1.a) and 3.12, 3.14 (Model 1.b). Due to the large dimension of the data, every submodel is further divided in tracer (tables 3.11 and 3.12) and tracee (tables 3.13 and 3.14) parameters. All parameters were estimated with good precision, as the maximum CV% is 41%.

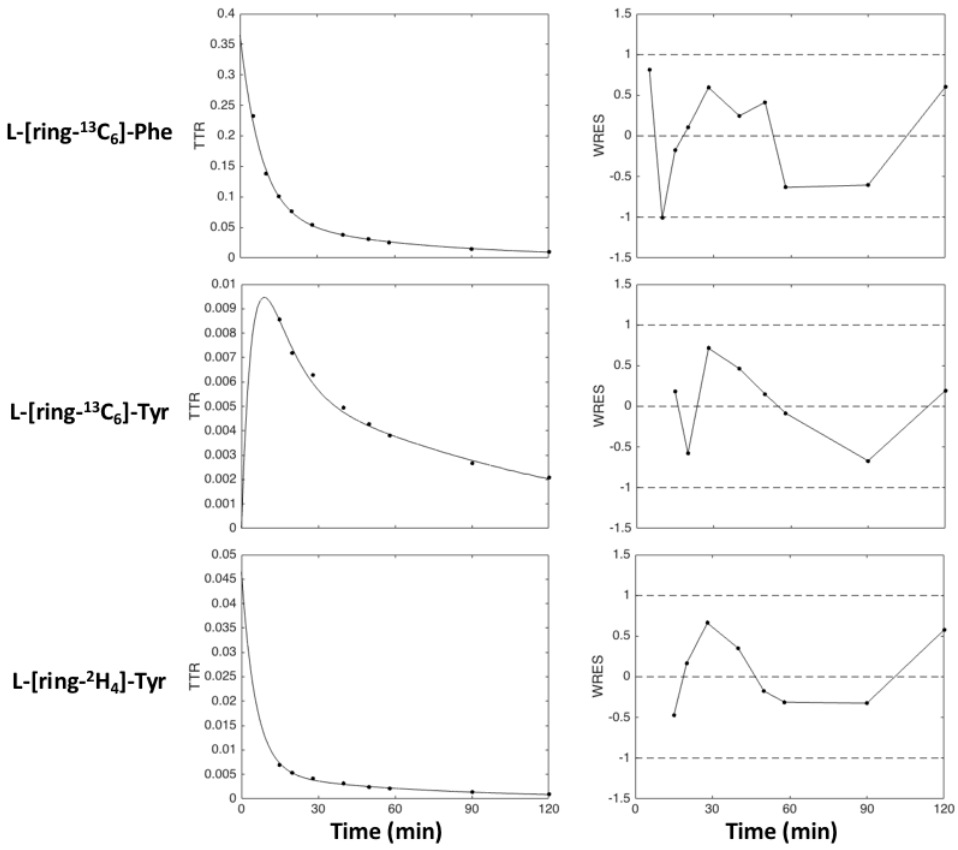

Figure 3.4: Ability of Model 1 to fit data

Average Data (solid dots) vs. Average model fit (continuous line) in left panels, average weighted residuals in right panels.

Table 3.10: Model 1 parameters

Variable	Unit	Lower Bound	Upper Bound
k_{01}	min^{-1}	0	0.051 ± 0.010
k_{02}	min^{-1}	0	0.019 ± 0.002
k_{03}	min^{-1}	0	0.079 ± 0.014
k_{04}	min^{-1}	0	0.017 ± 0.002
k_{12}	min^{-1}	0.017 ± 0.004	0.036 ± 0.006
k_{21}	min^{-1}	0.044 ± 0.007	0.095 ± 0.014
k_{31}	min^{-1}	0.0047 ± 0.0015	
k_{34}	min^{-1}	0.017 ± 0.006	0.033 ± 0.007
k_{43}	min^{-1}	0.076 ± 0.026	0.155 ± 0.033
Q_1	μmol	876 ± 196	
	μmol/FFM kg	16 ± 4	
Q_2	μmol	1095 ± 308	5503 ± 1919
	μmol/FFM kg	19 ± 4	94 ± 17
Q_3	μmol	475 ± 151	
	μmol/FFM kg	8 ± 3	
Q_4	μmol	1051 ± 330	4517 ± 1869
	μmol/FFM kg	19 ± 6	77 ± 21
F_{01}	μmol·FFM kg^{-1}·h^{-1}	0	46.4 ± 4.8
F_{02}	μmol·FFM kg^{-1}·h^{-1}	0	105.4 ± 12.3
F_{03}	μmol·FFM kg^{-1}·h^{-1}	0	38.4 ± 7.5
F_{04}	μmol·FFM kg^{-1}·h^{-1}	0	76.1 ± 15.2
F_{12}	μmol·FFM kg^{-1}·h^{-1}	40.8 ± 10.1	91.3 ± 14.2
F_{21}	μmol·FFM kg^{-1}·h^{-1}	40.8 ± 10.1	87.2 ± 13.9
F_{31}	μmol·FFM kg^{-1}·h^{-1}	4.1 ± 1.0	
F_{34}	μmol·FFM kg^{-1}·h^{-1}	38.3 ± 17.0	72.7 ± 22.2
F_{43}	μmol·FFM kg^{-1}·h^{-1}	38.3 ± 17.0	76.8 ± 22.6
U_1	μmol·FFM kg^{-1}·h^{-1}	0	50.2 ± 5.2
U_2	μmol·FFM kg^{-1}·h^{-1}	0	109.5 ± 12.6
U_3	μmol·FFM kg^{-1}·h^{-1}	0	34.3 ± 6.8
U_4	μmol·FFM kg^{-1}·h^{-1}	0	72.0 ± 14.4

Values are expressed as Mean ± SEM

Table 3.11: Model 1.a tracer parameters

Subj.		Q_1	Q_3	k_{01}	k_{03}	k_{12}	k_{21}	k_{31}	k_{34}	k_{43}
A	Value	989	604	0.046	0.068	0.029	0.038	0.0052	0.027	0.051
	CV%	8	19	7	15	11	12	11	16	20
B	Value	1137	364	0.035	0.083	0.038	0.042	0.0024	0.035	0.076
	CV%	4	18	4	14	6	8	9	12	18
C	Value	1105	783	0.053	0.068	0.03	0.046	0.0053	0.024	0.057
	CV%	12	25	10	18	12	16	14	11	14
D	Value	901	472	0.054	0.091	0.029	0.038	0.0057	0.03	0.062
	CV%	5	20	4	14	6	7	8	8	12
E	Value	823	361	0.056	0.099	0.04	0.049	0.0053	0.033	0.075
	CV%	11	28	9	19	10	17	14	11	16
F	Value	446	225	0.062	0.097	0.039	0.056	0.0057	0.044	0.145
	CV%	10	41	8	34	7	12	12	15	30
I	Value	931	595	0.046	0.07	0.043	0.049	0.0046	0.041	0.09
	CV%	12	21	10	16	12	21	13	8	11
L	Value	984	481	0.059	0.082	0.031	0.04	0.0045	0.027	0.051
	CV%	11	39	9	26	11	15	17	13	19
M	Value	703	483	0.064	0.085	0.032	0.05	0.0072	0.028	0.067
	CV%	9	24	7	17	8	11	12	11	15
N	Value	868	495	0.036	0.055	0.044	0.035	0.0024	0.038	0.09
	CV%	5	20	4	17	8	12	7	12	22
Q	Value	746	360	0.053	0.072	0.037	0.039	0.0029	0.041	0.077
	CV%	7	22	6	17	8	12	9	9	19
Mean	Value	876	475	0.051	0.079	0.036	0.044	0.0047	0.033	0.076
	CV%	9	25	7	19	9	13	11	12	18
	SEM	196	151	0.01	0.014	0.006	0.007	0.0015	0.007	0.026

Values are in min^{-1} (k_{ij}), μmol (Q_i). Precisions of estimated parameters are expressed as CV% = 100 SD($p_{i,est}$)/$p_{i,est}$, where CV is the coefficient of variation and SD is the standard deviation.

Table 3.12: Model 1.b tracer parameters

Subj.		Q_1	Q_3	k_{02}	k_{04}	k_{12}	k_{21}	k_{31}	k_{34}	k_{43}
A	Value	989	604	0.016	0.015	0.013	0.085	0.0052	0.012	0.119
	CV%	8	19	9	15	13	9	11	19	17
B	Value	1137	364	0.017	0.018	0.021	0.077	0.0024	0.017	0.159
	CV%	4	18	5	11	8	6	9	15	15
C	Value	1105	783	0.016	0.013	0.014	0.099	0.0053	0.011	0.126
	CV%	12	25	10	10	16	13	14	13	16
D	Value	901	472	0.017	0.018	0.012	0.093	0.0057	0.012	0.153
	CV%	5	20	5	7	8	5	8	11	13
E	Value	823	361	0.021	0.019	0.019	0.105	0.0053	0.014	0.174
	CV%	11	28	7	8	14	12	14	16	17
F	Value	446	225	0.02	0.018	0.019	0.118	0.0057	0.026	0.241
	CV%	10	41	5	8	10	10	12	21	31
I	Value	931	595	0.021	0.018	0.022	0.095	0.0046	0.023	0.16
	CV%	12	21	8	4	16	15	13	11	13
L	Value	984	481	0.019	0.016	0.013	0.099	0.0045	0.01	0.133
	CV%	11	39	9	12	15	11	17	19	22
M	Value	703	483	0.018	0.016	0.014	0.114	0.0072	0.012	0.152
	CV%	9	24	6	9	10	8	12	14	15
N	Value	868	495	0.022	0.015	0.022	0.072	0.0024	0.024	0.146
	CV%	5	20	5	10	11	8	7	14	20
Q	Value	746	360	0.021	0.02	0.015	0.092	0.0029	0.021	0.148
	CV%	7	22	6	7	11	8	9	13	17
Mean	Value	876	475	0.019	0.017	0.017	0.095	0.0047	0.017	0.155
	CV%	9	25	7	9	12	10	11	15	18
	SEM	196	151	0.002	0.002	0.004	0.014	0.0015	0.006	0.033

Values are in min^{-1} (k_{ij}), μmol (Q_i). Precisions of estimated parameters are expressed as CV% = 100 SD($p_{i,est}$)/$p_{i,est}$, where CV is the coefficient of variation and SD is the standard deviation.

Table 3.13: Model 1.a tracee parameters

Subj.		F_{01}	F_{03}	F_{12}	F_{21}	F_{31}	F_{34}	F_{43}	Q_1	Q_2	Q_3	Q_4	U_1	U_3
A	Value	42.3	37.6	35	35	4.7	28.6	28.6	15	20	9	18	47.1	32.9
	CV%	3	7	7	7	7	11	11	8	8	19	15	2	7
B	Value	47	35.7	56.2	56.2	3.2	32.7	32.7	22	25	7	16	50.2	32.5
	CV%	1	7	5	5	7	13	13	4	4	18	13	1	7
C	Value	51.2	47.1	45	45	5.1	39.3	39.3	16	25	12	27	56.4	41.9
	CV%	4	8	9	9	8	15	15	12	9	25	15	3	8
D	Value	43.3	38.1	30.7	30.7	4.6	25.8	25.8	13	18	7	14	47.8	33.6
	CV%	2	7	4	4	7	13	13	5	5	20	12	2	7
E	Value	42.4	32.9	37.3	37.3	4	25	25	13	16	6	13	46.5	28.8
	CV%	3	10	9	9	9	20	20	11	6	28	15	3	10
F	Value	39.8	31.3	36.1	36.1	3.6	46.8	46.8	11	15	5	18	43.4	27.6
	CV%	3	9	7	7	9	23	23	10	5	41	12	2	9
I	Value	56.6	55.3	61.1	61.1	5.7	70.9	70.9	21	24	13	29	62.3	49.6
	CV%	3	5	12	12	7	13	13	12	7	21	6	3	5
L	Value	49.3	33.3	33.4	33.4	3.8	20.8	20.8	14	18	7	13	53	29.5
	CV%	3	13	9	9	13	26	26	11	8	39	24	3	14
M	Value	44.2	40.1	34	34	5	31.5	31.5	12	18	8	19	49.2	35.1
	CV%	3	8	7	7	7	15	15	9	6	24	14	3	8
N	Value	47.7	41.6	46.7	46.7	3.2	68.1	68.1	22	18	13	30	50.8	38.5
	CV%	1	5	8	8	5	10	10	5	4	20	8	1	5
Q	Value	46.1	29.9	33.6	33.6	2.5	32	32	15	15	7	13	48.6	27.4
	CV%	2	6	7	7	6	11	11	7	5	22	7	2	6
Mean	Value	46.4	38.4	40.8	40.8	4.1	38.3	38.3	16	19	9	19	50.5	34.3
	CV%	3	8	8	8	8	16	16	9	6	25	13	2	8
	SEM	4.8	7.5	10.1	10.1	1	17	17	4	4	3	7	5.2	6.8

Values are in μmol·FFM kg^{-1}·h^{-1} (F_{ij}, U_i) or μmol/FFM kg (Q_i). Precisions of calculated variables are expressed as CV%, where CV is the coefficient of variation.

Table 3.14: Model 1.b tracee parameters

Subj.		F_{02}	F_{04}	F_{12}	F_{21}	F_{31}	F_{34}	F_{43}	Q_1	Q_2	Q_3	Q_4	U_2	U_4
A	Value	99.3	80.8	82.1	77.4	4.7	61.5	66.3	15	105	9	88	104	76.1
	CV%	5	9	4	4	7	8	8	8	11	19	17	5	9
B	Value	89	71.2	106.4	103.2	3.2	65.2	68.4	22	86	7	66	92.2	68
	CV%	3	8	3	3	7	9	9	4	5	18	13	3	8
C	Value	115.5	97.2	101.3	96.2	5.1	81.2	86.4	16	120	12	122	120.6	92.1
	CV%	6	6	5	5	8	11	11	12	12	25	10	6	6
D	Value	110.7	87.7	78.6	74	4.6	59.4	64	13	109	7	81	115.2	83.2
	CV%	3	5	2	2	7	9	9	5	6	20	9	3	5
E	Value	95.3	70.9	83.7	79.7	4	53.8	57.9	13	75	6	64	99.4	66.8
	CV%	6	7	5	5	9	14	14	11	11	28	11	6	7
F	Value	87.7	49.7	79.6	75.9	3.6	74.4	78.1	11	71	5	47	91.3	46
	CV%	5	6	4	4	9	18	17	10	8	41	9	4	6
I	Value	114.2	93.9	123.4	117.7	5.7	120.5	126.2	21	92	13	88	119.9	88.3
	CV%	7	3	6	6	7	10	10	12	11	21	4	7	3
L	Value	127.4	80.7	86.5	82.7	3.8	50.3	54.1	14	114	7	82	131.2	76.9
	CV%	6	9	4	5	13	19	18	11	12	39	15	6	9
M	Value	108	84.7	83.2	78.2	5	66.7	71.6	12	100	8	90	113	79.8
	CV%	4	6	4	4	7	11	11	9	8	24	11	4	6
N	Value	99.5	65.2	97.5	94.4	3.2	106.6	109.7	22	75	13	74	102.6	62
	CV%	5	6	4	4	5	8	7	5	8	20	9	4	6
Q	Value	112.9	55.5	82.2	79.7	2.5	59.5	62	15	88	7	47	115.3	53
	CV%	5	6	3	3	6	8	8	7	9	22	9	5	6
Mean	Value	105.4	76.1	91.3	87.2	4.1	72.7	76.8	16	94	9	77	109.5	72
	CV%	5	6	4	4	8	11	11	9	9	25	11	5	6
	SEM	12.3	15.2	14.2	13.9	1	22.2	22.6	4	17	3	21	12.6	14.4

Values are in μmol·FFM kg^{-1}·h^{-1} (F_{ij}, U_i) or μmol/FFM kg (Q_i). Precisions of calculated variables are expressed as CV%, where CV is the coefficient of variation.

3.2.2 The Six Compartments Model (Model 2)

The model provides a good fit of experimental data, shown in Figure 3.5. In particular, the mean weighted residuals' patterns confirmed by visual inspection the goodness of the fit.
The population average of every parameter is reported in Table 3.15, while the single subject values are reported in tables 3.16, 3.17, 3.18 and 3.19. Due to the large dimension of the data, the presentation of the results is divided in tracer (tables 3.16 and 3.17) and tracee (tables 3.18 and 3.19) parameters. All parameters were estimated with good precision, as the maximum CV% is 27%.

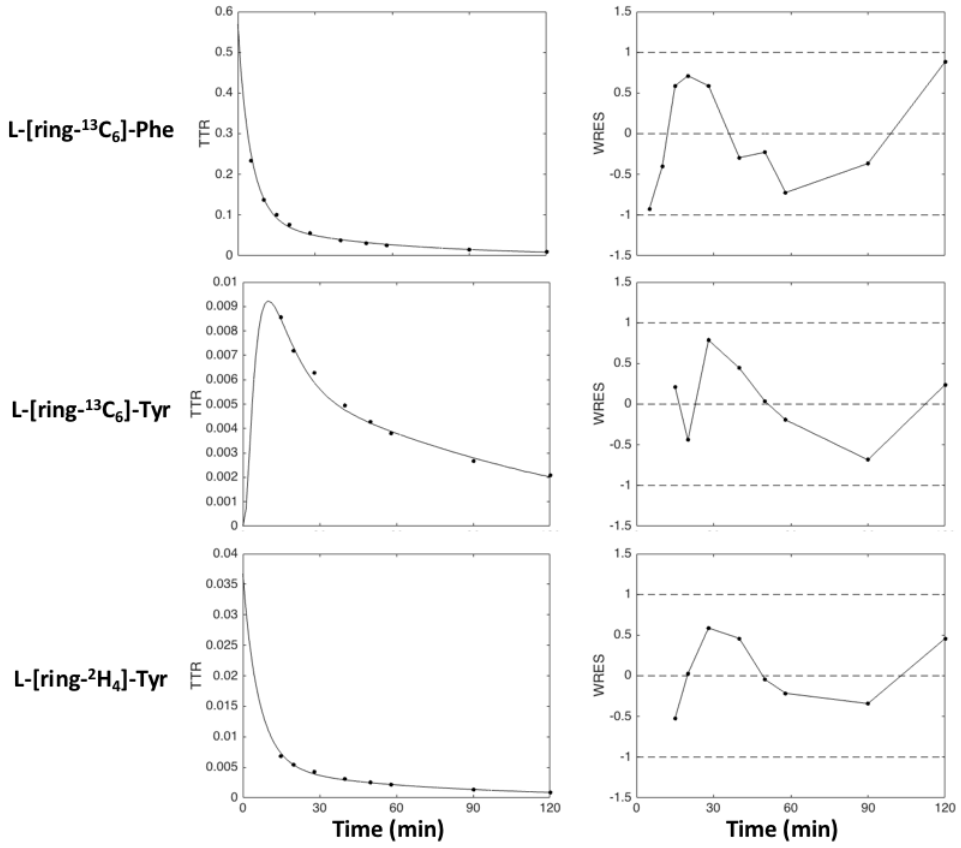

Figure 3.5: Ability of Model 2 to fit data

Average Data (solid dots) vs. Average model fit (continuous line) in left panels, average weighted residuals in right panels.

Table 3.15: Model 2 parameters

Variable	Unit	Value
k_{02}	min^{-1}	0.020 ± 0.003
k_{04}	min^{-1}	0.017 ± 0.002
k_{12}	min^{-1}	0.026 ± 0.016
k_{15}	min^{-1}	1.012 ± 0.004
k_{21}	min^{-1}	0.165 ± 0.055
k_{34}	min^{-1}	0.017 ± 0.006
k_{36}	min^{-1}	1.016 ± 0.004
k_{43}	min^{-1}	0.135 ± 0.032
k_{51}	min^{-1}	0.032 ± 0.0001
k_{63}	min^{-1}	0.017 ± 0.00001
k_{65}	min^{-1}	0.285 ± 0.082
Q_1	μmol	573 ± 165
	μmol/FFM kg	10 ± 2
Q_2	μmol	4459 ± 1867
	μmol/FFM kg	75 ± 19
Q_3	μmol	593 ± 195
	μmol/FFM kg	10 ± 2
Q_4	μmol	4806 ± 1976
	μmol/FFM kg	82 ± 22
Q_5	μmol	14 ± 4
	μmol/FFM kg	0.24 ± 0.05
Q_6	μmol	14 ± 4
	μmol/FFM kg	0.24 ± 0.04
F_{02}	μmol·FFM kg^{-1}·h^{-1}	89.5 ± 14.3
F_{04}	μmol·FFM kg^{-1}·h^{-1}	79.6 ± 15.1
F_{12}	μmol·FFM kg^{-1}·h^{-1}	102.7 ± 36.1
F_{15}	μmol·FFM kg^{-1}·h^{-1}	14.8 ± 2.9
F_{21}	μmol·FFM kg^{-1}·h^{-1}	98.7 ± 36.1
F_{34}	μmol·FFM kg^{-1}·h^{-1}	77.7 ± 16.4
F_{36}	μmol·FFM kg^{-1}·h^{-1}	14.4 ± 2.4
F_{43}	μmol·FFM kg^{-1}·h^{-1}	81.7 ± 16.6
F_{51}	μmol·FFM kg^{-1}·h^{-1}	18.9 ± 3.1
F_{63}	μmol·FFM kg^{-1}·h^{-1}	10.3 ± 2.0
F_{65}	μmol·FFM kg^{-1}·h^{-1}	4.0 ± 0.9
U_2	μmol·FFM kg^{-1}·h^{-1}	93.5 ± 14.8
U_4	μmol·FFM kg^{-1}·h^{-1}	75.6 ± 14.3

Values are expressed as Mean ± SEM

Table 3.16: Model 2 tracer parameters (Part 1)

Subject		k_{02}	k_{04}	k_{12}	k_{15}	k_{21}	k_{34}
A	Value	0.017	0.015	0.016	1.010	0.120	0.012
	CV%	10	17	14	13	6	21
B	Value	0.019	0.017	0.034	1.012	0.172	0.015
	CV%	10	20	17	13	9	27
C	Value	0.017	0.013	0.015	1.016	0.120	0.012
	CV%	10	14	15	13	6	17
D	Value	0.018	0.018	0.013	1.009	0.118	0.013
	CV%	8	6	11	13	4	10
E	Value	0.022	0.018	0.021	1.010	0.138	0.016
	CV%	8	9	14	13	6	15
F	Value	0.021	0.018	0.021	1.010	0.167	0.031
	CV%	7	9	13	13	6	20
I	Value	0.023	0.017	0.048	1.022	0.282	0.020
	CV%	9	3	22	12	14	6
L	Value	0.021	0.016	0.016	1.009	0.147	0.010
	CV%	10	13	17	13	7	17
M	Value	0.019	0.016	0.015	1.008	0.145	0.014
	CV%	7	9	11	13	4	13
N	Value	0.025	0.014	0.062	1.018	0.256	0.022
	CV%	8	10	19	13	13	14
Q	Value	0.023	0.020	0.021	1.010	0.151	0.022
	CV%	9	8	16	13	7	15
Mean	Value	0.020	0.017	0.026	1.012	0.165	0.017
	CV%	9	11	15	13	7	16
	SEM	0.003	0.002	0.016	0.004	0.055	0.006

Values are in min^{-1} (k_{ij}). Precisions of estimated parameters are expressed as CV% = 100 SD($p_{i,est}$)/$p_{i,est}$, where CV is the coefficient of variation and SD is the standard deviation.

Table 3.17: Model 2 tracer parameters (Part 2)

Subject		k_{36}	k_{43}	k_{51}	k_{63}	k_{65}
A	Value	1.015	0.104	0.032	0.017	0.293
	CV%	13	8	12	13	21
B	Value	1.016	0.116	0.032	0.017	0.167
	CV%	13	10	13	13	21
C	Value	1.022	0.106	0.031	0.017	0.275
	CV%	12	6	13	13	21
D	Value	1.015	0.131	0.032	0.017	0.316
	CV%	13	4	13	13	21
E	Value	1.013	0.117	0.032	0.017	0.336
	CV%	13	6	12	13	22
F	Value	1.015	0.188	0.032	0.017	0.358
	CV%	13	12	12	13	22
I	Value	1.023	0.187	0.031	0.017	0.366
	CV%	12	3	13	13	23
L	Value	1.012	0.110	0.032	0.017	0.284
	CV%	13	6	12	13	22
M	Value	1.011	0.154	0.032	0.017	0.399
	CV%	13	5	12	13	22
N	Value	1.020	0.162	0.031	0.017	0.174
	CV%	13	8	13	13	20
Q	Value	1.016	0.110	0.032	0.017	0.172
	CV%	13	7	12	13	20
Mean	Value	1.016	0.135	0.032	0.017	0.285
	CV%	13	7	13	13	21
	SEM	0.004	0.032	0.0001	0.00001	0.082

Values are in min^{-1} (k_{ij}). Precisions of estimated parameters are expressed as CV% = 100 SD($p_{i,est}$)/$p_{i,est}$, where CV is the coefficient of variation and SD is the standard deviation.

Table 3.18: Model 2 tracee parameters (Part 1)

Subject		F_{02}	F_{04}	F_{12}	F_{15}	F_{21}	F_{34}	F_{36}	F_{43}	F_{51}	F_{63}	F_{65}
A	Value	88.1	83.9	82.9	15.9	78.3	65.8	15.9	70.4	20.6	11.3	4.6
	CV%	5	6	6	16	6	8	9	8	12	13	5
B	Value	72.7	77.9	128.5	19.7	125.3	69.1	13.6	72.4	22.9	10.4	3.2
	CV%	5	8	9	15	9	11	10	10	13	13	6
C	Value	108.9	101.9	99.6	19.5	94.3	93.1	20.8	98.3	24.8	15.5	5.3
	CV%	5	6	6	16	6	6	9	6	13	13	5
D	Value	100.7	92.8	76.5	14.7	71.9	68.4	13.9	73.0	19.2	9.3	4.6
	CV%	4	3	4	17	4	4	9	4	13	13	3
E	Value	85.7	80.4	82.1	13.3	77.6	68.6	14.8	73.0	17.7	10.4	4.4
	CV%	4	4	6	17	6	6	9	6	12	13	5
F	Value	78.0	52.3	76.6	10.2	73.0	88.9	11.8	92.5	13.8	8.2	3.6
	CV%	4	4	5	17	6	12	9	12	12	13	5
I	Value	82.6	91.6	176.3	14.0	171.2	106.3	15.0	111.3	19.1	9.9	5.0
	CV%	6	2	14	17	14	4	9	3	13	13	6
L	Value	109.8	86.4	82.9	13.2	79.1	57.5	13.0	61.2	17.0	9.3	3.7
	CV%	6	5	6	16	7	6	9	6	12	13	7
M	Value	99.3	84.4	80.2	11.8	75.5	71.2	12.9	75.8	16.4	8.2	4.7
	CV%	4	4	4	17	4	5	8	5	12	13	4
N	Value	66.1	63.0	161.3	16.6	158.5	100.5	13.5	103.4	19.4	10.6	2.8
	CV%	5	4	13	15	13	8	10	8	13	13	5
Q	Value	92.3	61.0	83.0	14.4	80.5	65.4	12.7	67.8	16.8	10.3	2.4
	CV%	5	4	7	15	7	7	10	7	12	13	4
Mean	Mean	89.5	79.6	102.7	14.8	98.7	77.7	14.4	81.7	18.9	10.3	4.0
	CV%	5	4	7	16	7	7	9	7	13	13	5
	SEM	14.3	15.1	36.1	2.9	36.1	16.4	2.4	16.6	3.1	2.0	0.9

Values are in μmol·FFM kg^{-1}·h^{-1} (F_{ij}). Precisions of calculated variables are expressed as CV%, where CV is the coefficient of variation.

Table 3.19: Model 2 tracee parameters (Part 2)

Subject		Q_1	Q_2	Q_3	Q_4	Q_5	Q_6	U_2	U_4
A	Value	11	84	11	94	0.26	0.26	92.7	79.3
	CV%	0	10	0	15	20	15	4	7
B	Value	12	63	10	78	0.32	0.22	75.9	74.6
	CV%	0	10	0	19	19	16	5	8
C	Value	13	110	15	129	0.32	0.34	114.2	96.6
	CV%	0	11	0	12	20	16	5	6
D	Value	10	95	9	85	0.24	0.23	105.3	88.2
	CV%	0	9	0	7	21	15	4	3
E	Value	9	66	10	74	0.22	0.24	90.1	76.0
	CV%	0	10	0	10	21	15	4	4
F	Value	7	61	8	48	0.17	0.19	81.7	48.7
	CV%	0	9	0	10	21	15	4	5
I	Value	10	61	10	88	0.23	0.24	87.6	86.6
	CV%	0	12	0	3	21	15	6	2
L	Value	9	89	9	91	0.22	0.21	113.6	82.6
	CV%	0	13	0	13	21	16	6	5
M	Value	9	88	8	87	0.19	0.21	104.0	79.8
	CV%	0	8	0	9	22	15	3	4
N	Value	10	43	11	77	0.27	0.22	69.0	60.2
	CV%	0	10	0	8	19	16	5	4
Q	Value	9	67	10	50	0.24	0.21	94.7	58.6
	CV%	0	11	0	10	19	16	5	4
Mean	Mean	10	75	10	82	0.24	0.24	93.5	75.6
	CV%	0	10	0	11	20	16	5	5
	SEM	2	19	2	22	0.05	0.04	14.8	14.3

Values are in μmol/FFM kg (Q_i) or μmol·FFM kg^{-1}·h^{-1} (U_i) . Precisions of calculated variables are expressed as CV%, where CV is the coefficient of variation.

Chapter 4

Discussion and validation

4.1 The Four Compartments Model (Model 1)

4.1.1 Model overview

The 4 compartments proposed model is not a priori uniquely identifiable, meaning that its 9 k_{ij}'s and 2 Q_i's cannot be uniquely determined from the data. This is due to the fact that since protein synthesis and breakdown take place in all tissues, it is not possible to exclude a priori the presence of any of the irreversible losses (k_{0i}) and productions (U_i) in both compartments of Phe and Tyr kinetics. Moreover, it is not possible to establish constraints between the parameters, once we come up with the physiological meaning of every compartment. In fact, since we assume that both compartments 1 and 3 represent the plasma + fast exchanging tissues pool (for Phe and Tyr, respectively), we must assume that some Phe or Tyr is being disposed towards protein synthesis or oxidation (in the case of Tyr). Same fact holds for compartments 2 and 4, that represent the slow tissues pool (for Phe and Tyr, respectively). Although the model is not uniquely identifiable, we can estimate uniquely only some combinations of the rate constants. Hence, only the kinetic parameters that can be expressed as a function of the observational parameters can be calculated uniquely: Q_1, Q_3 and k_{31}. For the other parameters, only the interval of admissible values can be obtained, basing the analysis on the use of submodels (Model 1.a and Model 1.b) [19, 10]. Adopting this technique, each submodel is both a priori and a posteriori identifiable, meaning that all of its parameters can be estimated with very good precision from the experimental data (CV%'s never exceed 41%). The estimations from each submodel constitute the range of admissible values for every parameter of the original system model.

4.1.2 Model development and rationale

The model proposed has the least number of compartments required to account for the dynamic properties of our data and to be consistent with known physiology. The disappearance of both tracers in plasma can be described by a two-term exponential equation (sections 2.2 and 3.1), indicating that there is at least one compartment equilibrating the plasma pool over the studied period for each amino acid [36]. One may argue that this compartment should be the intracellular pool alone, where the conversion from Phe to Tyr is known to be taking place [26]. Even though this may seem the most physiologically attractive option (Model 7, Figure 4.2), the attempt to fit experimental data to a model with such structure failed to describe the appearance in plasma of Tyr as Phe's metabolite (Figure 4.1). This failure to fit data with that simple model structure suggests that the exchanges between plasma and the intracellular pool (in which the hydroxylation process is happening) might be so fast that it is not possible to model the pools as separate compartments. This appears to be consistent with the studies of Thompson [35] and Layman [23], where it is also speculated that the pool for Phe hydroxylation might mix extremely rapidly with the body pool. Therefore, it was chosen to locate the site of conversion from Phe to Tyr directly in the accessible compartments (1 and 3), thus merging plasma and fast exchanging tissues in one single pool. In the spirit of such consideration, the most logical (and physiologically based) suggestion for the other compartment to be equilibrating with plasma (and fast tissues all together, at this point) appears to be the slow exchanging tissues compartment (compartments 2 and 4, Figure 2.1).

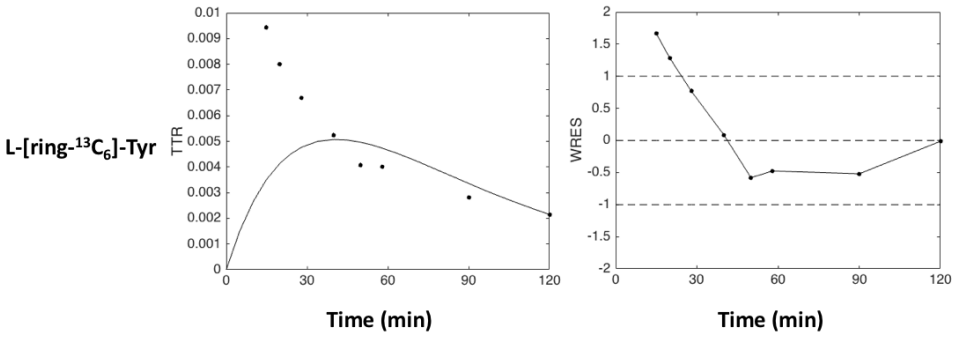

Figure 4.1: Failure to describe L-[ring-$^{13}C_6$]-Tyr data with Model 7

Data (solid dots) vs. model fit (continuous line) in left panel, weighted residuals in right panel (from Subject A).

Keeping in mind that this model structure has a clear physiological relevance, the issue of the *a priori* identifiability of the tracer model is not easy to overcome. As already mentioned before, it is not easy to establish a

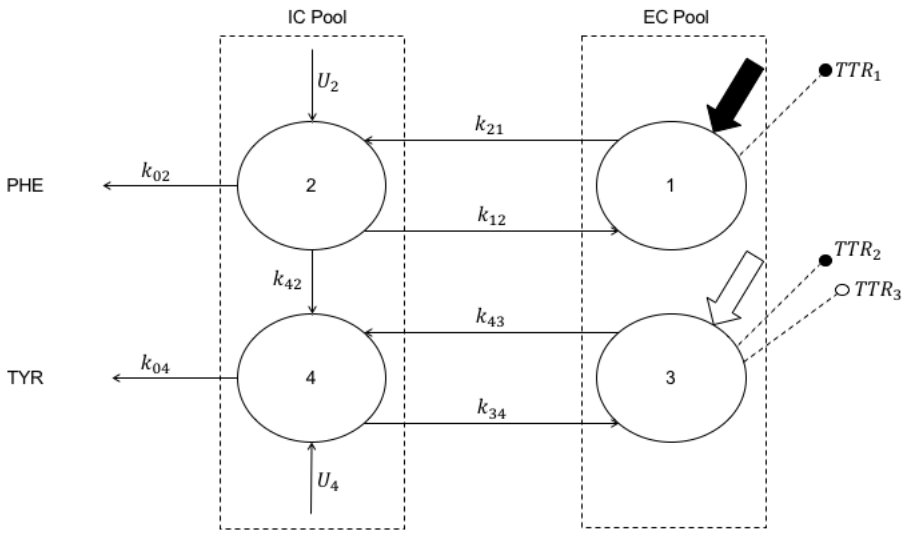

Figure 4.2: Model 7 structure

The circles indicate compartments representing kinetically distinct pools of Phenylalanine and Tyrosine and the arrows between them the intercompartmental fluxes. k_{ij} (per minute) are the transfer rate constants of flux from compartment j to compartment i. Large arrows denote Phe (solid arrow) and Tyr (open arrow) tracer inputs. TTR_i measurements are indicated by dashed lines ending with solid (from Phe tracer input) or open (from Tyr tracer input) circle, respectively.

constraint for the two irreversible losses (k_{01}, k_{02} and k_{03}, k_{04}) in the compartments of each amino acid, as it would have the effect of making the tracer model uniquely identifiable. Additional complications arise from the assumption that compartments 1 and 3 merge two physiologically known to be distinct pools [26], so that using constraints such as $k_{01} = k_{02}$ and $k_{03} = k_{04}$ would be difficult to justify. Based on these considerations, it was decided not to use any constraints of such kind and to proceed by identifying bounds for the parameters of this non-uniquely identifiable model. This approach is meant to give the reader a less biased overview of the underlying physiological system, by making the least number of possible assumptions. Finally, just as one cannot exclude a priori the existence of the irreversible losses (k_{0i}), it is not trivial to establish the site from which the amino acids are entering the system by protein breakdown. In fact, one would probably observe protein catabolism in both slow and fast exchanging tissues during the study period. Therefore, it was chosen to break the main model into submodels once again, in order to establish the upper and lower bounds for the fluxes of interest in the tracee model.

4.1.3 Model features

An important feature of the model is that the hydroxylation flux (F_{31}) is uniquely identifiable from the dataset and is estimated with very high precision (averaging a CV% of 8% for the 11 subjects, tables 3.13 and 3.14). In general, one would expect the variables $R_{a,Phe}$, $R_{a,Tyr}$ and $Phe \rightarrow Tyr$ of the non-compartmental analysis [36] to match the variables U_1, $U_3 + F_{31}$ and F_{31} (respectively) provided by Model 1.a of the compartmental analysis. This is indeed verified when $R_{a,Phe}$, $R_{a,Tyr}$ and $Phe \rightarrow Tyr$ are obtained from AUCs from Model 1 fitted curves. Nevertheless, these values show differences with the pure non-compartmental analysis (sections 2.2 and 3.1), as resumed in Table 4.1.

Table 4.1: Comparison for relevant physiological variables as computed by non-compartmental approaches and the minimal compartmental approach

Approach		AUC_{Phe+6}	AUC_{Tyr+4}	AUC_{Tyr+6}	$R_{a,Phe}$	$R_{a,Tyr}$	$Phe \rightarrow Tyr$
NC (Complete)	Mean	6.582	0.477	0.769	50.4	47.8	5.7
	SEM	1.593	0.150	0.181	4.9	9.0	1.5
NC (Partial)	Mean	6.582	0.501	0.759	50.4	44.5	5.2
	SEM	1.593	0.140	0.209	4.9	5.7	1.3
C (Model 1)	Mean	6.577	0.586	0.696	50.5	38.4	4.1
	SEM	1.662	0.167	0.175	5.2	7.5	1.0

Values are in min (AUC_{AA+i}), μmol·FFM kg^{-1}·h^{-1} ($R_{a,AA}$ and $Phe \rightarrow Tyr$). NC (Complete) column refers to the non-compartimental approach when all data points are considered, while NC (Partial) column represents the same approach when samples at t=5 and 10 minutes are discarded from Tyr curves. C (Model 1) column represents the computation of the variables from Model 1 fitted curves.

As one can see, $R_{a,Phe}$ computed from Model 1 curves remains perfectly consistent with the non-compartmental approach. On the other side, $R_{a,Tyr}$ shows a higher variability, depending on the approach adopted. In fact, the values computed with non-compartmental approaches are greater than their compartmental counterpart. Such observation is easily understandable by observing the comparison between the average fitted curves in Figure 4.3 (L-[ring-$^2H_4$]-Tyr, left panel): the TTR values at t=0 min provided by Model 1 are consistently higher than those given by the non-compartmental approaches (even when the first two samples are not considered).

The differences in the TTR values at t=0 min imply a systematically higher value for AUC_{Tyr+4} from Model 1 (0.586 ± 0.167 min, mean ± SEM) when compared to the non-compartmental approaches (0.477 ± 0.150 and 0.501 ± 0.586 min, respectively, mean ± SEM), resulting in a lower value for $R_{a,Tyr}$ from Model 1 (38.4 ± 7.5 μmol·FFM kg^{-1}·h^{-1}, mean ± SEM)

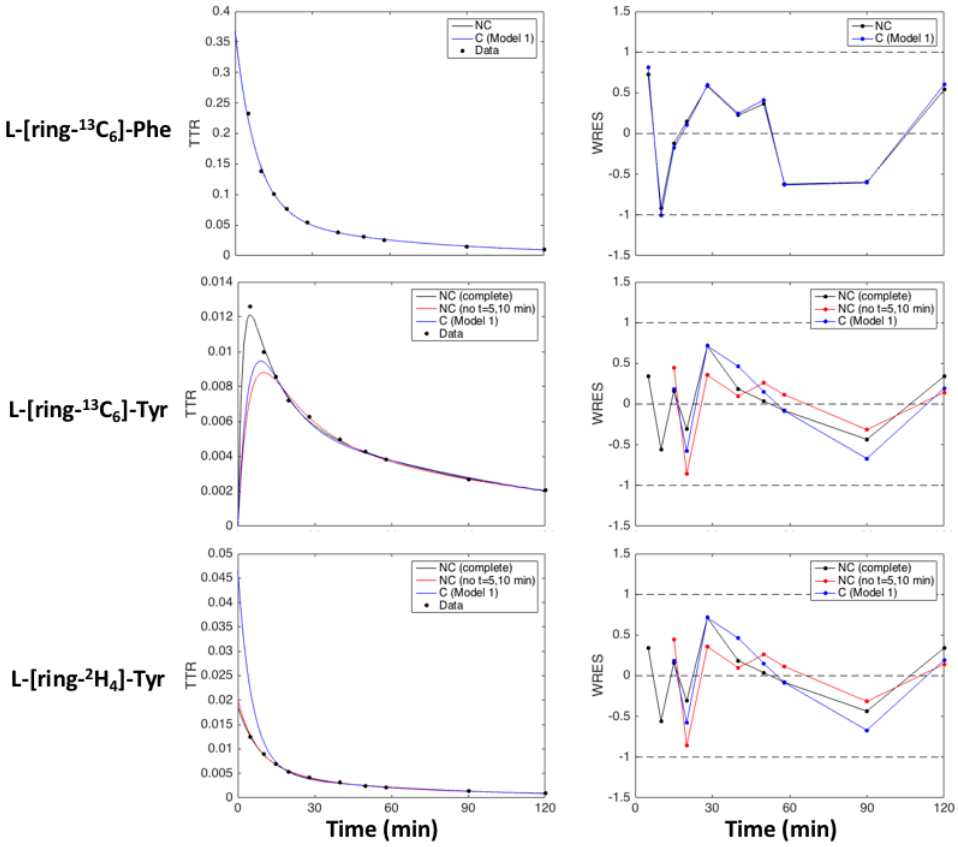

Figure 4.3: Comparison between non-compartmental and compartmental (Model 1) fitted curves

Average Data (solid dots) vs. Average model fit (continuous line) in left panels, average weighted residuals in right panels. Continuous blue line represents non-compartmental approach when all data points are considered, while the continuous red line represents the same approach when samples at t=5 and 10 minutes of Tyr curves are discarded. Continuous black line represents Model 1.

when compared to the NC approaches (47.8 ± 9.0 and 44.5 ± 5.7 μmol·FFM kg^{-1}·h^{-1}, respectively, mean ± SEM). Therefore, the effect of excluding Tyr samples at t=5 and 10 minutes from the analysis is not so determinant in terms of variability for $R_{a,Tyr}$, as one might expect; instead, it is the use of a compartmental approach that marks the biggest separation. Indeed, the Model 1 fitted curves are generated from kinetic parameters that use information from both L-[ring-^{2}H$_4$]-Tyr and L-[ring-^{13}C$_6$]-Tyr TTR curves and are therefore more physiologically relevant than the non-compartmental curves. Finally, the differences existing in the computed $Phe \rightarrow Tyr$ conver-

sion rates appear to be mainly due to the value of $R_{a,Tyr}$ as it is entered in equation (2.14). Nevertheless, by observing the intervals in terms of mean ± SEM provided by the three approaches one can see that they are overlapping, meaning consistency between the approaches.
At this point, it is interesting to compare the net PB (Protein Breakdown) flux of Model 1 (F_{31}) to the one obtained by Engelen et al. [18] with primed constant infusion of the isotopes L-[ring-$^2H_5$]-Phe and L-[ring-$^2H_2$]-Tyr in 11 healthy male subjects in the postabsorptive state (Table 4.2). The above mentioned study recorded a value of 4.6 ± 0.3 μmol·FFM kg^{-1}·h^{-1} (mean ± SEM) for the net PB flux, which is comparable to the 4.1 ± 1.0 μmol·FFM kg^{-1}·h^{-1} (mean ± SEM) predicted by Model 1. In addition, the values of PB (53.0 ± 2.7 μmol·FFM kg^{-1}·h^{-1} (mean ± SEM)) and PS (Protein Synthesis) (48.5 ± 2.5 μmol·FFM kg^{-1}·h^{-1} (mean ± SEM)) appear quite close to the those given by Model 1.a (50.5 ± 5.2 μmol·FFM kg^{-1}·h^{-1} (mean ± SEM) and 46.4 ± 4.8 μmol·FFM kg^{-1}·h^{-1} (mean ± SEM), respectively). These observations appear to confirm the quality of the variables as they are gleaned from the compartmental analysis in the present pulse protocol study.

Table 4.2: Comparison between variables gleaned from primed constant infusion (non-compartmental) [18] and pulse (compartmental) data

	Primed Const. Infusion (NC)	Pulse (C, Model 1.a)
PS	48.5 ± 2.5	46.4 ± 4.8
PB	53.0 ± 2.7	50.5 ± 5.2
Net PB	4.6 ± 0.3	4.1 ± 1.0

Values are in μmol·FFM kg^{-1}·h^{-1} (mean ± SEM). PS, PB stand for Protein Synthesis and Protein Breakdown, respectively. Data in the Primed Const. Infusion (NC) column were obtained with NC approach calculations in 11 male healthy subjects (postabsorptive state) by Engelen et al. [18] from primed constant infusion of isotopes L-[ring-$^2H_5$]-Phe and L-[ring-$^2H_2$]-Tyr. Data in the Pulse (C, Model 1.a) column were obtained in the present study by compartmental analysis for Model 1.a.

As mentioned in Section 2.3, another feature of the model is it underlines an important problem, namely: Tyr tracers might suffer from a mixing pool issue in the initial minutes after the pulse injection [21, 27]. Having a closer look at the plots displayed in Figure 3.4, one may observe that the samples at t=5 and 10 minutes are discarded from the analysis in the two Tyr curves. When it was attempted to fit the data (including these first two samples of the Tyr curves) to the model, it was recorded a trending underestimation of the L-[ring-$^2H_4$]-Tyr data in the first 3-4 samples (Figure 4.4), and that observation led to inspect the physiological feasibility of the accessible es-

timated pools: while Q_1 (967.64 $\pm$ 150.97 μmol) was estimated to be well above the threshold (approx. 136 μmol) for the minimum possible sampling plasma pool for Phe in every subject, Q_3 (124.62 $\pm$ 58.84 μmol) and its individual values for the majority of the subjects were estimated to be below the threshold (approx. 139 μmol) for the minimum possible sampling pool for Tyr, which leads to a physiologically infeasible system. The above considerations suggested that the first two Tyr samples might have been biased by the mixing issue related to the Tyr pool [21, 27], and as a result it was decided to discard those samples from the analysis.

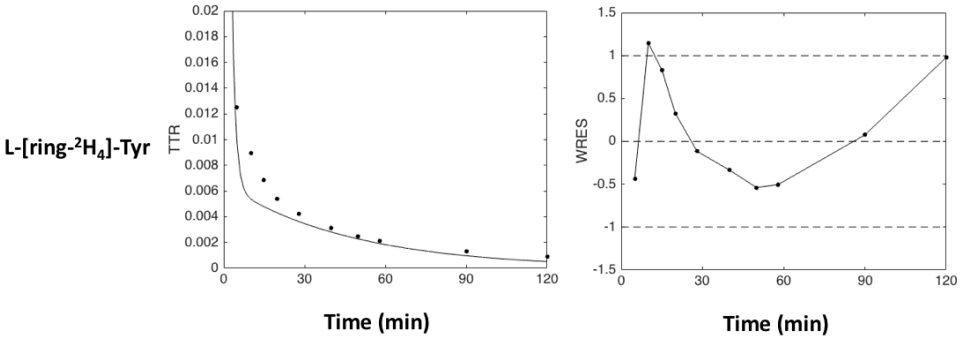

Figure 4.4: Systematic underestimation of the first samples in L-[ring-$^2H_4$]-Tyr data when samples at t=5 and 10 minutes are considered

Average Data (solid dots) vs. Average model fit (continuous line) in left panel, average weighted residuals in right panel.

4.1.4 Physiological evidence

As far as the uniquely estimable pools (Q_1 and Q_3) are concerned, the model allows for some interesting observations. It was already pointed out in Section 4.1.3 that if one considers the average $[Phe]_{plasma}$ (41 μmol/L), one can estimate the plasma Phe pool to be approximately 136 μmol (assuming the plasma volume to be a standard 3.3 L). Additionally, if one assumes Phe's concentration in the liver, which is responsible for the most part of the hydroxylation process occurring in the body, to be approximately double the concentration recorded in plasma, as supported by data in pigs (unpublished, courtesy of CTRAL), we would roughly have $[Phe]_{liver} = 82$ μmol/L. Assuming then a standard liver volume of 1.5 L [34], that allows to estimate the Phe mass in the liver to be around 123 μmol. In that sense, the sum of plasma and liver pools of Phe could be estimated to be roughly 259 μmol. At the same time, Model 1 estimates the average value for Q_1 to be approximately 876 μmol which would leave about 617 μmol of free Phe unassigned. The remaining portion of this big pool is likely to be constituted by extracellular fluids (437 μmol, if we do not account for the already considered plasma) and

other tissues in fast exchange with plasma (occupying the about remaining 180 μmol).
Using similar assumptions, we can estimate the plasma Tyr pool to be approximately 139 μmol (starting from an average $[Tyr]_{plasma}$(42 μmol/L)). Assuming then $[Tyr]_{liver}$ = 84 μmol/L, one can estimate the Tyr mass in the liver to be around 126 μmol, thus making the sum of plasma and liver pools of Tyr roughly 256 μmol. At the same time, the model estimates the average value for Q_3 to be approximately 475 μmol, which would leave about 210 μmol of free Tyr that is not trivial to assign. The remaining part of this pool is likely to be comprised mainly by a portion extracellular fluids and tissues in fast exchange with plasma. These considerations seem to confirm the physiological feasibility of the uniquely estimable pools provided by the model, given the fact that the concentrations of the two amino acids in the liver are unknown for the study subjects and may differ significantly from what is observed in pigs. It is interesting to notice how even though Q_1 and Q_3 are likely representative of analogous portions of the whole body and although the plasma concentrations of the two amino acids as an average are quite similar, the model estimates the two pools quite differently. This is likely to result from a faster Phe exchange with a larger portion of the body fluids and tissues compared to that of Tyr. It would be intriguing to test the model on Phe and Tyr tracer data obtained in humans either by pulse (with a more packed sampling scheme in the first 10 minutes) or by continuous infusion. In the latest case in particular, the mixing pool issue of Tyr for the first samples should not be present because the isotopic equilibrium would be achieved sometime during the study period: if the pool sizes of Q_1 and Q_3 would show a similar trend, then the aforementioned hypothesis would be empirically verified.
As far as the non-uniquely identifiable pools are concerned (Q_2 and Q_4) we can only provide the interval of validity of the masses of free Phe and Tyr they contain. One can notice how in both cases and for the average estimations on the population, the averages of the estimated upper and lower bounds (56.7 μmol/FFM kg for Q_2 and 48.1 μmol/FFM kg for Q_4, which should give the idea of the pools in a midway situation between the two limit case scenarios of models 1.a and 1.b) identify pools much bigger than the uniquely identifiable Q_1 (15.7 μmol/FFM kg) and Q_3 (8.5 μmol/FFM kg). This observation appears to be consistent with the assumption of appointing compartments 2 and 4 to tissues in slow exchange with plasma and fast tissues, since these would find their counterpart mainly in the muscles, physiologically known to be a much bigger pool than the content of compartments 1 and 3.
Another unique feature of the compartmental analysis is that we have two possible protein synthesis rates; the rate into the fast exchanging pool which could be the fast turnover protein and the rate into the slow exchanging pools. Because the model is not uniquely identifiable, only upper and lower

limits are provided. Nevertheless, Model 1.b is likely to better represent the changes in protein synthesis and breakdown in tissues like muscle. In fact, being the subjects of the study in postabsorptive state, in order to ensure the protection from degradation of the essential amino acids, the maximal activities of the enzymes responsible for the degradation of the amino acids in the liver are low, which could be translated in very limited or negligible amounts for protein breakdown/synthesis fluxes (U_1, U_3, F_{01} and F_{03}) for compartments 1 and 3 of Model 1. This hypothesis was later verified through the development of Model 2, as described in Section 4.2.6.

4.1.5 Consistency with the literature

The average endogenous productions (tables 3.13 and 3.14), entering the tracee system (U_1, U_2, U_3 and U_4), i.e. free Phe and Tyr coming from protein catabolism in the two limit cases provided by the two submodels (Figure 2.2) can be used to quantify the ratio $\frac{P_t}{P_p}$, which is the molar ratio of the fluxes of Tyr and Phe arising from protein catabolism. Animal studies [29] in the past estimated this ratio from protein composition to be 0.73 and a study of Thompson et al. [35] recorded a ratio of 0.76 in human subjects with a Phe-based non-compartmental model. In the case of Model 1.a, where both the endogenous productions and the disposals are located in the plasma + fast tissues pools (compartments 1 and 3), average estimated values of 50.5 ± 5.2 μmol·FFM kg^{-1}·h^{-1} (mean ± SEM) were recorded for Phe entering the system from protein breakdown (U_1) and of 34.3 ± 6.8 μmol·FFM kg^{-1}·h^{-1} (mean ± SEM) for Tyr entering the system by the same process (U_3), thus returning a value of $\frac{P_t}{P_p}$ of 0.68. In the case of Model 1.b, where both the endogenous productions and the disposals are located in the slow tissues pools (compartments 2 and 4), average estimated values of 109.5 ± 12.6 μmol·FFM kg^{-1}·h^{-1} (mean ± SEM) were recorded for Phe entering the system from protein breakdown (U_2) and of 72.0 ± 14.4 μmol·FFM kg^{-1}·h^{-1} (mean ± SEM) for Tyr entering the system by the same process (U_4), thus returning a value of $\frac{P_t}{P_p}$ of 0.66. Keeping in mind that the most likely physiological situation might be the one in which both fast and slow tissues have protein breakdown happening, the limit cases of the molar ratio $\frac{P_t}{P_p}$ recorded by Model 1 in the two scenarios are consistent with previously published results. The two recorded molar ratios in the two limit scenarios displayed by the here presented compartmental model (0.68 and 0.66, respectively for Model 1.a and 1.b) appear to be consistent with the observations of Matthews [26], where it is reported that the expected rate of Tyr from protein breakdown to be ∼0.60 that of Phe.

Furthermore, the study performed by Cortiella et al. [14] with a non compartmental approach in the postabsorptive state reported that approximately 14% of Tyr flux is derived from Phe hydroxylation, while the rate of Phe that gets hydroxylated is approximately 11%. If one considers Model 1.a,

the scenario that is closer in terms of structural similarities to the non-compartmental approach, one would notice that the submodel reports that approximately 12% of Tyr flux is derived from Phe hydroxylation, while the rate of Phe that gets hydroxylated is approximately 8%. This shows how with Model 1.a, because of the structural similarities with the non-compartmental approach, we get estimates somehow consistent with those obtained through non-compartmental approaches published in the literature, with rates reported by compartmental analysis systematically slightly lower, but with the benefit of a deeper structural insight. To be fair, all previously published models could not glean the actual rates of protein breakdown in the slow exchanging tissues, which are likely to better represent the whole body protein physiology than the plasma rates of appearance, so that making a comparison is not possible. For this reason, it is important to remark how by choosing a model structure (Model 1.a) in which the endogenous productions are located in the accessible compartments, the obtained values are somehow consistent with values published in the literature, even though Model 1.b is would probably better describe the actual kinetics of Phe-Tyr metabolism in the postabsorptive state. The validation of Model 2 appears to back up this hypothesis, as described in Section 4.2.6.

4.2 The Six Compartments Model (Model 2)

4.2.1 Model overview

The 6 compartments proposed model is *a priori* uniquely identifiable, meaning that its 11 k_{ij}'s can be uniquely determined from the data. Since samples at t=5 and 10 minutes of Tyr curves were not considered and the model structure is more complex than Model 1 (accounting for 2 compartments more), the accessible pool sizes Q_1 and Q_3 were calculated *a priori*, starting from the fat-free mass (FFM) and plasma concentrations of Phe and Tyr of every subject, as described in Section 2.3.2. Furthermore, *maximum likelihood* (ML) estimation of some of the unknown parameters (k_{15}, k_{36}, k_{51} and k_{63}) was not possible and therefore *maximum a priori* (MAP) estimation was used for such kinetic parameters.
The aim of this model is to overcome the identifiability issue provided by the previously described four compartments model (Model 1), in order to provide a more detailed and complete picture of Phe-Tyr metabolism kinetics. The model allows the accurate description of all unknown kinetic parameters (as CV%'s do not exceed 27%) and was later validated by simulating a continuous infusion experiment previously performed in pigs on the mean human subject with it.

4.2.2 Model development and rationale

It was already mentioned how 2 is the minimum number of compartments per amino acid that allows the assessment of Phe-Tyr kinetics. Nevertheless, merging the plasma compartments and those responsible for the hydroxylation process (fast exchanging tissues) leads to unidentifiability of the minimal model structure because of the reasons that were presented in Section 4.1.1. In the six compartments model (Model 2) here discussed, protein breakdown and synthesis of Phe and Tyr in the sites responsible for the conversion (compartments 5 and 6) were assumed to be negligible, so as Tyr oxidation was. The reason for such choice is to be found in CTRAL's unpublished data from a pig study, obtained by using a continuous infusion protocol. In fact, taking a look at Table 4.3 that resumes this study, one can see how the $\frac{TTR_L}{TTR_P}$ (where subscripts L and P stand for liver and plasma, respectively) ratio of Phe at the steady state is close to 1, while the $\frac{TTR_L}{TTR_P}$ ratio of Tyr in the same condition is higher than that value.

Table 4.3: Statistics of $\frac{TTR_L}{TTR_P}$ ratio in CTRAL's unpublished pig study data

	$\frac{TTR_L}{TTR_P}$
Phe	0.98 ± 0.26
Tyr	2.70 ± 1.22

Values are Mean ± SEM and were calculated at the steady state with a constant infusion protocol

These data suggest that free Phe in plasma and liver (the latest being the site mainly responsible for hydroxylation [26]) might be able to achieve isotopic equilibrium at the steady state, meaning that from none of these compartments there are endogenous productions entering the system. At the same time, these data hint how between free Tyr in liver and plasma there is no isotopic equilibrium, but this is due to the portion of Tyr that is converted from Phe in the liver. In fact, being the subjects of the study in postabsorptive state, in order to ensure the protection from degradation of the essential amino acids, the maximal activities of the enzymes responsible for the degradation of the amino acids in the liver are known to be low. Because protein breakdown of Phe in the liver appears to be negligible, it is reasonable to assume that also protein breakdown and oxidation of Tyr can be overlooked. These informations were translated to Model 2 structure: compartments 1 and 3 are therefore representative of plasma and EC fluid, physiologically unable to breakdown or synthetize proteins [26]; compartments 5 and 6 represent the IC portion of tissues responsible for the

hydroxylation process, in which protein breakdown and synthesis fluxes are assumed to be negligible.
Because of these physiologically based assumptions, the entering site (via protein breakdown) in the model for free Phe and Tyr are compartments 2 and 4, respectively (U_2 and U_4). Similarly, the protein synthesis process (with Tyr oxidation, for Compartment 4) is assumed to take place in the same two compartments (F_{02} and F_{04}). These compartments represent the IC portion of tissues exchanging with a slower kinetics with the accessible EC pools (compartments 1 and 3).

4.2.3 Model features

As already pointed out, the key feature of Model 2 is that every unknown parameter is uniquely identifiable from the dataset, once the previously mentioned assumptions are made. Furthermore, every parameter is estimated with very high precision (maximum CV% is 27%), also due to the use of MAP estimation for some of the unknown parameters (k_{15}, k_{36}, k_{51} and k_{63}). The hydroxylation flux (F_{65}) of Model 2, assumes a value (4.0 ± 0.9 μmol·FFM kg^{-1}·h^{-1}, mean ± SEM) in line to the one (F_{31}) estimated by Model 1 (4.1 ± 1.0 μmol·FFM kg^{-1}·h^{-1}, mean ± SEM). This fact somehow appears to confirm the physiological feasibility of the structural assumptions made, even more when we consider what the possible consequences of moving the endogenous productions (U_5, U_6) and the disposals (k_{05}, k_{06}) to the compartments involved in the hydroxylation process would be: F_{65} equal to 59.3 ± 20.3 μmol·FFM kg^{-1}·h^{-1} (mean ± SEM), which would be much higher than Model 1 results and the conversion rates present in the literature [26, 18].
Moreover, arguably the most innovative feature of Model 2 is that it allows for the assessment of the actual protein breakdown rate of Phe in tissues, rather than just an indication of it, as the $R_{a,Phe}$ provided by the non-compartmental approaches does. In fact, $R_{a,Phe}$ measures only a portion of the entire breakdown rate of Phe in tissues and the assessment of such quantity is not possible with non-compartmental approaches. Therefore, it is not possible to make a comparison with values provided by the literature either. Nevertheless, it is interesting to notice how the PB rate in tissues (U_2) provided by Model 2 is 93.5 ± 14.8 μmol·FFM kg^{-1}·h^{-1} (mean ± SEM), which is almost as double as the $R_{a,Phe}$ calculated from the L-[ring-$^{13}C_6$]-Phe curve (Model 1 fit, Table 4.1). This is something physiologically expected, because of the aforementioned reasons.

4.2.4 Physiological evidence

Estimating *a priori* the accessible EC pools (Q_1 and Q_3), allows to identify all the remaining ones (Q_2, Q_4, Q_5 and Q_6) as IC pools by exclusion. This appears to strengthen the physiological relevance of the protein breakdown

and synthesis rates from Phe (U_2 and F_{02}) as they are provided by Model 2. As far as the estimated pools are concerned, the model allows for some interesting observations. Q_2 and Q_4 are higher (75 ± 19 and 82 ± 22 μmol/FFM kg, mean $\pm$ SEM, respectively) than their EC counterparts Q_1 and Q_3 (both $10 \pm 2 \pm \mu$mol/FFM kg, mean $\pm$ SEM). This seems to be consistent with the interpretation previously given to the slow tissues compartments of the model: in fact, if we assume that compartments 2 and 4 represent mainly muscular tissue, then this big difference is feasible, because the concentrations of Phe and Tyr in muscle are likely to be higher than those in plasma (Table 1.2), along with the muscles being a very large portion of the body. Similarly, it is interesting to have a look (Table 3.15) at the estimated values for Q_5 and Q_6: these pools are considerably small in size (0.24 ± 0.05 and 0.24 ± 0.04 μmol/FFM kg, mean $\pm$ SEM, respectively), probably because only a coherently small portion of the liver is involved in the Phe to Tyr conversion.
As far as the gleaned fluxes are concerned, the model allows for some further interesting observations. First of all, looking at the average values for F_{15}, F_{36}, F_{51} and F_{63} (Table 3.15), one can see how the EC pools (compartments 1 and 3) exchange with the IC pools involved in the hydroxylation process (compartments 5 and 6) with a very fast kinetics, especially if the sizes of these compartments are considered. In fact, looking at the average fractional transfer rates (Table 3.15) k_{15}, k_{36}, k_{51} and k_{63}, one can see how the pools responsible for hydroxylation mix extremely rapidly with the EC pools. This appears to be consistent with the studies of Thompson [35], Layman [23] and what was observed in the development of Model 1: the exchanges between these pools are so rapid that it is particularly complicated to model them as separate entities. On the other end, if one observes the average fluxes F_{12}, F_{21}, F_{34} and F_{43} (Table 3.15), it is possible to see how even though these are higher than F_{15}, F_{36}, F_{51} and F_{63}, the pools involved (Q_1, Q_2, Q_3 and Q_4) are in general way bigger in size than Q_1, Q_3, Q_5 and Q_6, thus denoting a lower specific activity. Therefore, this observation is consistent with the interpretation that was given to compartments 2 and 4: they are representative of a very large IC portion of tissues in slow exchange with the EC pools and the sites responsible for hydroxylation of Phe.

4.2.5 Consistency with the literature

The average endogenous productions (Table 3.15) entering the tracee system (U_2 and U_4), i.e. free Phe and Tyr coming from protein catabolism in slow tissues, can be used to quantify the ratio $\frac{P_t}{P_p}$, which is the molar ratio of the fluxes of Tyr and Phe arising from protein catabolism. It was already mentioned in Section 4.1.5 how animal studies [29] in the past estimated this ratio from protein composition to be 0.73, while a study of Thompson et al. [35] recored a ratio of 0.76 in human subjects with a Phe-based non-

compartmental model. In the case of Model 2, average estimated values of 93.5 ± 14.8 μmol·FFM kg^{-1}·h^{-1} (mean ± SEM) for Phe entering the system from protein breakdown (U_2) and of 75.6 ± 14.3 μmol·FFM kg^{-1}·h^{-1} (mean ± SEM) for Tyr entering the system by the same process (U_4) were recorded, thus returning a value of $\frac{P_t}{P_p}$ of 0.81. Therefore, the molar ratio $\frac{P_t}{P_p}$ recorded by Model 2 is somehow consistent with the previously published results.
Since all models regarding Phe-Tyr metabolism present in the literature are based on non-compartmental approaches, it is not possible to make any further comparisons similarly to what was done for Model 1.a. Nevertheless, the value of the hydroxylation flux (F_{65}, 4.0 ± 0.9 μmol·FFM kg^{-1}·h^{-1}, mean ± SEM) provided by Model 2 appears to be quite consistent with the results of Engelen et al. [18] in a similar study group obtained with a primed constant infusion protocol (4.6 ± 0.3 μmol·FFM kg^{-1}·h^{-1}, mean ± SEM).

4.2.6 *In silico* validation

The average estimated tracer parameters shown in Table 3.15 were used to validate Model 2 through the simulation of a previously performed experiment in pigs by the CTRAL. The original pigs experiment used a continuous infusion protocol of the stable isotopes L-[ring-$^{13}C_6$]-Phe and L-[3,3-D_2]-Tyr. The study involved 21 pigs and the infusion rates for the isotopes were of 56.6 ± 1.7 nmol·BW kg^{-1}·min^{-1} (mean ± SEM, L-[ring-$^{13}C_6$]-Phe) and 53.1 ± 2.3 nmol·BW kg^{-1}·min^{-1} (mean ± SEM, L-[3,3-D_2]-Tyr). The average infusion rate of every stable isotope solution was proportioned to the mean human subject body weight (85.9 BW kg) and used as input in the simulation software SAAM II (version 2.2.1), together with the average kinetic parameters shown in tables 3.15. At the steady state, TTRs in compartments 1, 3, 5 and 6 were assessed (TTR_1, TTR_3, TTR_5 and TTR_6, respectively) and $\frac{TTR_5}{TTR_1}$, $\frac{TTR_6}{TTR_3}$ were computed. These ratios were later compared to the $\frac{TTR_L}{TTR_P}$ ratios of Phe and Tyr found in pigs. The comparison is resumed in Table 4.4.

Table 4.4: Comparison between real pig and human simulated data (mean subject, Model 2)

Phe		Tyr	
$\frac{TTR_L}{TTR_P}$ (Pig)	$\frac{TTR_5}{TTR_1}$ (Human)	$\frac{TTR_L}{TTR_P}$ (Pig)	$\frac{TTR_6}{TTR_3}$ (Human)
0.98 ± 0.26	1	2.70 ± 1.22	3.49

Values are adimensional (ratio), mean ± SEM in the $\frac{TTR_L}{TTR_P}$ columns

As one can notice, the values obtained with the *in silico* simulation are quite similar to the ones provided by the pig study, if we account for the

possible interspecies differences existing. The simulation appears to confirm the validity of the structural assumptions made in the design phase, together with the physiological relevance of the model. The fact that at the steady state real pig and simulated human data show good consistency, suggests that compartments 5 and 6 of the model might be well representative of the IC portion of the liver. Furthermore, these results appear to confirm how the scenario provided by Model 1.b might be the most physiologically relevant in Model 1, given the similar structural assumptions made.

Chapter 5

Conclusions

In summary, two compartmental models of Phenylalanine (Phe) and Tyrosine (Tyr) metabolism in healthy subjects were developed, by using two stable isotope tracer pulses administered intravenously. Kinetic analysis was performed on the three tracer responses in plasma expressed by tracer-tracee ratios and obtained by LC-MS/MS by isotope dilution. As far as the simplest model (Model 1) is concerned, even though some of the variables of the model are not a priori identifiable, it provides an important and physiologically sound overview of Phe and Tyr metabolism (in terms of intervals of validity) than the non-compartmental approaches presented in the past, making the least number of possible structural assumptions. One of the limit case scenarios (Model 1.a) described by this model shows results that are compatible with those found using less structurally complex approaches. Nevertheless, the other limit case scenario (Model 1.b) is likely to be better representative of changes in protein synthesis and breakdown in tissues like muscle, thanks to the development of a more complex and detailed compartmental model (Model 2). This last model provides accurate estimates for all the unknown parameters, gathers innovative and detailed structural informations for the metabolism of Phe-Tyr kinetics and was validated by simulating a continuous infusion experiment previously done on pigs. The models also allowed the identification of an issue related to the mixing properties of the accessible Tyr pool in the first minutes after the pulse injection, not detectable by means of non-compartmental approaches.
The models presented in this thesis could serve not only as as a useful reference for a more complete and physiologically based overview of the Phe and Tyr metabolic pathways but it could also guide future developments in the modeling of amino acids characterized by resembling structural properties. By describing the postabsorptive whole body protein kinetics in healthy humans, the models provide a direction to accurately and comprehensively assess alterations in whole body protein synthesis and breakdown rates in disease states.

Bibliography

[1] Naji N Abumrad, David Rabin, Michael P Diamond, and William W Lacy. Use of a heated superficial hand vein as an alternative site for the measurement of amino acid concentrations and for the study of glucose and alanine kinetics in man. *Metabolism*, 30(9):936–940, 1981.

[2] P Hugh R Barrett, Bradley M Bell, Claudio Cobelli, Hellmut Golde, Alan Schumitzky, Paolo Vicini, and David M Foster. SAAM II: simulation, analysis, and modeling software for tracer and pharmacokinetic studies. *Metabolism*, 47(4):484–492, 1998.

[3] Giuseppina Bellu, Maria Pia Saccomani, Stefania Audoly, and Leontina D'Angiò. DAISY: a new software tool to test global identifiability of biological and physiological systems. *Computer methods and programs in biomedicine*, 88(1):52–61, 2007.

[4] Dennis M Bier. Intrinsically difficult problems: the kinetics of body proteins and amino acids in man. *Diabetes/metabolism reviews*, 5(2):111–132, 1989.

[5] Gianni Biolo, David Chinkes, Xiao-Jun Zhang, and Robert R Wolfe. Harry M. Vars Research Award: a new model to determine in vivo the relationship between amino acid transmembrane transport and protein kinetics in muscle. *Journal of Parenteral and Enteral Nutrition*, 16(4):305–315, 1992.

[6] Wayne T Buckley, Stuart N Huckin, and Guenter K Eigendorf. Calculation of stable isotope enrichment for tracer kinetic procedures. *Biological Mass Spectrometry*, 12(1):1–5, 1985.

[7] Ewart R Carson, C Cobelli, and L Finkelstein. The mathematical modeling of metabolic and endocrine systems: model formulation, identification, and validation. *AMC*, 10:12, 1983.

[8] Joe TR Clarke and Dennis M Bier. The conversion of phenylalanine to tyrosine in man. Direct measurement by continuous intravenous tracer infusions of L-[ring-$^{2}H_{5}$] phenylalanine and L-[1-^{13}C] tyrosine in the postabsorptive state. *Metabolism*, 31(10):999–1005, 1982.

[9] Claudio Cobelli and JJ DiStefano. Parameter and structural identifiability concepts and ambiguities: a critical review and analysis. *American Journal of Physiology-Regulatory, Integrative and Comparative Physiology*, 239(1):R7–R24, 1980.

[10] Claudio Cobelli, David Foster, and Gianna Toffolo. *Tracer kinetics in biomedical research*, volume 1. Springer Science & Business Media, 2000.

[11] Claudio Cobelli, MP Saccomani, Paolo Tessari, Gianni Biolo, Livio Luzi, and Dwight E Matthews. Compartmental model of leucine kinetics in humans. *American Journal of Physiology-Endocrinology and Metabolism*, 261(4):E539–E550, 1991.

[12] Claudio Cobelli, Gianna Toffolo, Dennis M Bier, and Roman Nosadini. Models to interpret kinetic data in stable isotope tracer studies. *American Journal of Physiology-Endocrinology And Metabolism*, 253(5):E551–E564, 1987.

[13] Claudio Cobelli, Gianna Toffolo, and David M Foster. Tracer-to-tracee ratio for analysis of stable isotope tracer data: link with radioactive kinetic formalism. *American Journal of Physiology-Endocrinology And Metabolism*, 262(6):E968–E975, 1992.

[14] Joaquin Cortiella, J Sergio Marchini, Steven Branch, Thomas E Chapman, and Vernon R Young. Phenylalanine and tyrosine kinetics in relation to altered protein and phenylalanine and tyrosine intakes in healthy young men. *The American journal of clinical nutrition*, 56(3):517–525, 1992.

[15] H-Ch Curtius, JA Völlmin, and K Baerlocher. The use of deuterated phenylalanine for the elucidation of the phenylalanine-tyrosine metabolism. *Clinica Chimica Acta*, 37:277–285, 1972.

[16] H-Ch Curtius, MJ Zagalak, K Baerlocher, J Schaub, W Leimbacher, and U Redweik. In vivo studies of the phenylalanine-4-hydroxylase system in hyperphenylalaninemics and phenylketonurics. *Helvetica paediatrica acta*, 32(6):461–469, 1978.

[17] Dominique Darmaun, Dwight E Matthews, and Dennis M Bier. Physiological hypercortisolemia increases proteolysis, glutamine, and alanine production. *American Journal of Physiology-Endocrinology And Metabolism*, 255(3):E366–E373, 1988.

[18] MPKJ Engelen, AM Safar, T Bartter, F Koeman, and NEP Deutz. High anabolic potential of essential amino acid mixtures in advanced nonsmall cell lung cancer. *Annals of Oncology*, page mdv271, 2015.

[19] KR Godfrey and JJ DiStefano III. Identifiability of model parameters. *Identifiability of parametric models*, pages 1–20, 1987.

[20] Hanns-Dieter Grümer, Hans Koblet, and Carol Woodard. Phenylalanine metabolism in the phenylpyruvic condition. II. An attempt to calculate the daily incorporation of phenylalanine into proteins. *Journal of Clinical Investigation*, 41(1):61, 1962.

[21] WP James, PJ Garlick, PM Sender, and JC Waterlow. Studies of amino acid and protein metabolism in normal man with L-[U-^{14}C] tyrosine. *Clinical science and molecular medicine*, 50(6):525–532, 1976.

[22] JC King and RJ Cousins. Modern nutrition in health and disease. *Modern Nutrition in Health Disease, SM ME, Ross AC, Caballero B, Cousins RJ (eds) pp*, pages 271–285, 2005.

[23] Donald K Layman and Robert R Wolfe. Sample site selection for tracer studies applying a unidirectional circulatory approach. *American Journal of Physiology-Endocrinology and Metabolism*, 253(2):E173–E178, 1987.

[24] Yvette C Luiking, Martijn Poeze, and Nicolaas E Deutz. Arginine infusion in patients with septic shock increases nitric oxide production without haemodynamic instability. *Clinical Science*, 128(1):57–67, 2015.

[25] R Matalon, DE Matthews, K Michals, and D Bier. The use of deuterated phenylalanine for the in vivo assay of phenylalanine hydroxylase activity in children. *Journal of inherited metabolic disease*, 5(1):17–19, 1982.

[26] Dwight E Matthews. An overview of phenylalanine and tyrosine kinetics in humans. *The Journal of nutrition*, 137(6):1549S–1555S, 2007.

[27] Lyle L Moldawer, Isao Kawamura, Bruce R Bistrian, and George L Blackburn. The contribution of phenylalanine to tyrosine metabolism in vivo. studies in the post-absorptive and phenylalanine-loaded rat. *Biochemical Journal*, 210(3):811–817, 1983.

[28] AR Moss, Rudolf Schoenheimer, et al. The conversion of phenylalanine to tyrosine in normal rats. *Journal of Biological Chemistry*, 136:415–429, 1940.

[29] HN Munro and A Fleck. Analysis of tissues and body fluids for nitrogenous constituents. *Mammalian protein metabolism*, 3:423–525, 1969.

[30] Eric Newsholme and Anthony Leech. *Functional biochemistry in health and disease*. John Wiley & Sons, 2011.

[31] John A Rathmacher, Paul J Flakoll, and Steven L Nissen. A compartmental model of 3-methylhistidine metabolism in humans. *American Journal of Physiology-Endocrinology and Metabolism*, 269(1):E193–E198, 1995.

[32] Anthony San Pietro, D Rittenberg, et al. A study of the rate of protein synthesis in humans. II. Measurement of the metabolic pool and the rate of protein synthesis. *Journal of Biological Chemistry*, 201:457–473, 1953.

[33] Noel F Shambaugh, Howard B Lewis, Dee Tourtellotte, et al. Comparative studies of the metabolism of the amino acids. 4. Phenylalanine and tyrosine. *Journal of Biological Chemistry*, 92:499–511, 1931.

[34] Kenji Suzuki, Ryan Kohlbrenner, Mark L Epstein, Ademola M Obajuluwa, Jianwu Xu, and Masatoshi Hori. Computer-aided measurement of liver volumes in CT by means of geodesic active contour segmentation coupled with level-set algorithms. *Medical physics*, 37(5):2159–2166, 2010.

[35] GN Thompson, PJ Pacy, H Merritt, GC Ford, MA Read, KN Cheng, and D Halliday. Rapid measurement of whole body and forearm protein turnover using a [$^2H_5$] phenylalanine model. *American Journal of Physiology-Endocrinology And Metabolism*, 256(5):E631–E639, 1989.

[36] Robert R Wolfe and David L Chinkes. *Isotope tracers in metabolic research: principles and practice of kinetic analysis*. John Wiley & Sons, 2005.

List of Figures

List of Tables

Aknowledgements

I would like to express my gratitude to my supervisor Professor Gianna M Toffolo, PhD for the useful comments, remarks, engagement through the learning process of this master thesis and for giving me the opportunity to explore the World while doing a job I loved. Furthermore, I would like to thank my co-supervisor Professor Nicolaas EP Deutz, PhD, MD for the precious dataset, along with useful comments, suggestions and last but not least for opening a world of professional opportunities to me. Also, I would like to thank Sunday Simbo, PhD for coordinating the study, Amy Heiner and Liz Martinez, RN for assisting the subjects during the study, John J Thaden, PhD for performing the sample analysis, all the subjects who have participated in this research and every member of the CTRAL for the continuous support and making me feel like home during my days with them. I would like to thank my loved ones, who have supported me throughout entire process, by giving me the strength I thought I didn't have. Thanks to my wonderful parents, for always teaching me by example and not just by words. Finally, a special thanks goes to my girlfriend Serena, for enlightening my life from the first second she walked into it. I will be grateful forever for your love.